Received: 4 May 2024 | Revised: 26 February 2025 | Accepted: 9 April 2025

DOI: 10.1002/qj.4999

Quarterly Journal of the Royal Meteorological Society RMetS

RESEARCH ARTICLE

Too-stable North Atlantic climate system in CMIP6 experiments undermines precipitation projections in Europe

A. Halifa-Marín[1,2,3] | M. A. Torres-Vázquez[3,4] | R. Trigo[5] | S. M. Vicente-Serrano[1,2] | M. Turco[3] | P. Jiménez-Guerrero[3] | J. P. Montávez[3]

[1]Instituto Pirenaico de Ecología, Consejo Superior de Investigaciones Científicas (IPE–CSIC), Zaragoza, Spain

[2]Laboratorio de Climatología y Servicios Climáticos (LCSC), CSIC-Universidad de Zaragoza, Zaragoza, Spain

[3]Department of Physics, Regional Atmospheric Modelling Group, Regional Campus of International Excellence Campus Mare Nostrum, University of Murcia, Murcia, Spain

[4]Environmental Remote Sensing Research Group, Department of Geology, Geography and Environment, Universidad de Alcalá, Alcalá de Henares, Spain

[5]Instituto Dom Luiz, Faculdade de Ciências, Universidade de Lisboa, Lisbon, Portugal

Correspondence
Amar Halifa-Marín, Instituto Pirenaico de Ecología, Consejo Superior de Investigaciones Científicas (IPE–CSIC), Zaragoza, Spain.
Email: amar.halifa@ipe.csic.es

Funding information
Spanish Ministry of Science, Innovation and Universities–Agencia Estatal de Investigación and the European Regional Development Fund, Grant/Award Numbers: PID2020-115693RB-I00, PID2021-123193OB-I00; Spanish Ministry of Science, Innovation and Universities, Grant/Award Number: FPU18/00824; Ramón y Cajal Grant, Grant/Award Number: RYC2019-027115-I

Abstract

This study investigates fluctuations in the spatial pattern of the North Atlantic Oscillation (NAO) during the Industrial Era. NAO variability was analyzed over successive 30-year periods, clustering its spatial patterns using two metrics: the gradient (g) between its action centres and flux direction (fd). Three distinct NAO patterns were identified, each exhibiting significant implications for NAO–precipitation modulation in the North Atlantic region. Coupled Model Intercomparison Project (CMIP6) climate models were evaluated for their ability to replicate these observed patterns. While many models accurately reproduce all three patterns, they frequently misinterpret their frequencies, favouring a disproportionately stable NAO. This bias, consistent across historical, natural-only, and greenhouse gas forcings (GHG only), as well as piControl simulations, appears intrinsic to the models. This misinterpretation is significantly reduced in ssp585 scenarios, suggesting a potential link between forcing levels and improved multidecadal NAO variability in models. The occurrence of those different NAO patterns introduces uncertainty in precipitation projections, as this bias can persist in future scenarios. These findings highlight the need for improved model representation of NAO spatial variability to enhance the reliability of precipitation projections, particularly for Europe.

KEYWORDS

CMIP6 models, large-scale circulation patterns, North Atlantic climate, North Atlantic Oscillation

1 | INTRODUCTION

Winter climate variability in the North Atlantic sector is predominantly driven by the North Atlantic Oscillation (NAO). The NAO is characterized by alternating (seesaw) changes in sea level pressure (SLP) between, for example, the Azores (subtropical North Atlantic region) and Iceland (Arctic North Atlantic). Its influence on the Northern Hemisphere's climate is derived by two NAO phases (Hurrell *et al.*, 2003). The positive phase (NAO+) features an intensified jet stream and a northward-shifted storm track, resulting in mild, wet winters in northern Europe and cold, dry conditions in southern Europe. In contrast, NAO− exhibits inverse dynamics and synoptic patterns, albeit with some asymmetries.

This description reflects the canonical characteristics of the NAO commonly recognized in the literature. However, several studies have revealed significant temporal and spatial variability in the NAO (e.g., Börgel *et al.*, 2020; Moore *et al.*, 2013; Wang *et al.*, 2012). The NAO's spatial pattern is non-stationary, exhibiting substantial multidecadal and centennial fluctuations. These changes manifest as mobility in the latitude and longitude of its action centres – regions with dominant SLP anomalies displaying opposite behaviour. This spatial variability is particularly relevant because different NAO patterns result in significant variations in associated climate conditions across Europe (e.g., Comas-Bru & McDermott, 2014; Hu *et al.*, 2022; Vicente-Serrano & López-Moreno, 2008). Such variability may contribute to extreme events, including droughts, floods, heatwaves, cold spells, and winter storms (Fuentes-Franco *et al.*, 2023; Lehmann & Coumou, 2015; Oltmanns *et al.*, 2020; Tsanis & Tapoglou, 2019).

Despite advancements in understanding the mechanisms driving the NAO (e.g., Omrani *et al.*, 2022; Singh *et al.*, 2018; Woollings *et al.*, 2015), a comprehensive framework for identifying the factors that trigger and modulate its long-term variability remains elusive. This gap hampers predictive capabilities (Christiansen *et al.*, 2022; Eade *et al.*, 2022). Moreover, the non-stationary nature of the NAO complicates the interpretation of historical climate records and challenges efforts to disentangle natural variability from anthropogenic influences on observed climate changes (Hu *et al.*, 2022; Schurer *et al.*, 2023; Smith *et al.*, 2020). Discrepancies among historical NAO reconstructions further highlight these challenges (Hernández *et al.*, 2020).

The IPCC Sixth Assessment Report (AR6) (Eyring *et al.*, 2021; Gulev *et al.*, 2021, and references therein) acknowledges that uncertainties in the long-term variability of the NAO persist in the latest generation of the Coupled Model Intercomparison Project (CMIP6). While CMIP6 models reliably reproduce the canonical spatial pattern, explained variance, and teleconnections of the NAO with high confidence, they fail to capture its long-term variability. This limitation persists despite incremental improvements across model generations since CMIP3 (Fasullo *et al.*, 2020).

State-of-the-art literature thus suggests that while most models can interpret the full range of NAO variability, they do not fully replicate shifts of its action centres and trend, which still represents a significant achievement in climate simulations. This limitation raises the hypothesis that simulations may inadequately represent NAO spatial patterns, their frequencies and persistence. Given that NAO-induced climate impacts are closely tied to its spatial configurations, the inability to accurately capture its long-term variability could introduce substantial uncertainties in European precipitation projections. In response to the challenge posed by AR6 to improve understanding of the NAO's long-term variability and to differentiate its response to anthropogenic warming from natural variability, this study aims to:

1. Characterize the observed structures of the NAO pattern and evaluate their implications for winter precipitation in Europe.
2. Assess the ability of CMIP6 datasets to capture the spatial configurations of the NAO, including their observed magnitude and persistence.
3. Attribute the spatial patterns of the NAO to natural forcing or greenhouse gas (GHG) forcing.
4. Examine how accurately simulating changes in the NAO's spatial patterns influences precipitation projections over Europe.

Therefore, this work addresses the variability and shifts in the NAO pattern while evaluating the performance of CMIP6 simulations in representing these dynamics.

2 | DATA AND METHODS

2.1 | Sources of climate data

2.1.1 | Reanalysis and observations

Monthly SLP and precipitation rate fields were sourced from the 20CRv3 reanalysis (80-member; Slivinski *et al.*, 2021) for the period 1851–2014. This dataset represents the most temporally extensive surface-input reanalysis, incorporating more and higher-quality observations and offering enhanced spatial resolution (T254; $1° \times 1°$ grid). The ECMWF ERA20C (Poli *et al.*, 2016) and ERA5 (Hersbach *et al.*, 2020) reanalyses, as well as the NCEP reanalysis (Kalnay *et al.*, 1996), were also

used to assess differences between datasets. Additionally, observed monthly precipitation data were included using a European dataset of rain gauges comprising 199 series. This dataset exhibits minimal missing data for the period 1851–1870 and provides complete time series from 1871 to 2014 (Vicente-Serrano *et al.* Vicente-Serrano *et al.*, 2021). These observational series are also employed to evaluate the reliability of the monthly precipitation data generated by the 20CRv3 reanalysis. Additionally, it used the Greenland Blocking (GB) Index based on Geopotential Height at 500 hPa from 20CRv2c and NCEP reanalyses, following Hanna *et al.* (2016), and the Atlantic Multidecadal Oscillation Index (AMO) based on Sea Surface Temperature (SST) from the ERSST dataset (Huang *et al.*, 2017), according to the Trenberth and Shea (2006) methods.

2.1.2 | Climate models

Simulated monthly data of SLP and precipitation were retrieved from the Multi-Model Large Ensemble Archive (MMLEA) version 1, which provides a large number of CMIP6 simulations for the historical, ssp245, and ssp585 scenarios (Deser *et al.*, 2020). This selection also includes high-resolution realizations from CNRM-CM6-1 and MPI-ESM1-2, as well as ACCESS-ESM1-5 and MIROC-ES2L. A total of 462 historical simulations were provided by 11 models, incorporating all the observed natural and anthropogenic forcings. A total of 287 simulations were analyzed for the ssp245 scenario and 262 for the ssp585 scenario, which features greater incremental forcing. Additionally, 173 historical natural-only (hist-nat) and 159 historical greenhouse gas only (hist-GHG) simulations were analyzed to examine climate variability sensitivity to natural and anthropogenic forcings. The hist-nat simulations are forced solely by solar and volcanic activity, while hist-GHG simulations include only increased GHG. Echoing the IPCC AR6 conclusions (Eyring *et al.*, 2021), 29 amip-hist simulations were evaluated to assess whether the atmosphere–ocean coupling modulates the long-term variability of the NAO in climate models. These historical simulations assume all forcings but prescribe SST by ocean nudging using the HadISST dataset (Rayner *et al.*, 2003). The last 165 years of a piControl simulation for each model/realization were analyzed (18), covering a duration like the historical period (1850–2014). Those simulations serve as a baseline against which perturbation experiments are evaluated. Table 1 clarifies all the CMIP6 runs used in the study. More technical details about the utilized CMIP6 runs are presented in the implemented protocol documentation (CMIP, 2024). Finally, a small set of historical CMIP5 simulations (26, see Table S1) grouped in the MMLEA (Deser *et al.*, 2020), was also used to compare variations between the two most recent CMIP projects.

2.2 | Analysis and statistical methods

2.2.1 | Data preparation

All gridded data were interpolated onto a grid with a spatial resolution of $1° \times 1°$, adopted from the 20CRv3 reanalysis. Average or accumulation for the canonical winter (December–February) were computed. Comparative analyses between piControl, historical, hist-nat, and hist-GHG simulations with 20CRv3 were carried out for the common period (1851–2014; year is for January). Conversely, the analysis comparing amip-hist with 20CRv3 is constrained by the temporal coverage of the HasISST dataset (1871–2014). Similarly, comparisons between future scenarios (2016–2100) and 20CRv3 involve periods of different lengths.

2.2.2 | Computation of the NAO features in numerous periods

The NAO is defined as the leading empirical orthogonal mode (EOF) by applying Singular Value Decomposition (SVD) to spatially weighted (i.e., square root of the cosine of latitude) winter SLP anomalies by subtracting the full-period average (step 1 in Figure 1, see Equations S1–S4). This statistical method follows the procedures outlined in Campitelli *et al.* (2022) and its R code (Campitelli, 2021) for detection of leading modes of climate variability, which provides the spatial pattern and temporal variations of principal components (PC), as well as their relative importance in the decomposition (explained variance; EV). The SVD is applied on the spatial domain framed in 90° W–40° E, 20–80° N, following Hurrell *et al.*'s (2003) definition for NAO.

We identified the mode of variability corresponding to NAO in as many 30-year running periods as possible (1851–1880, 1852–1881 so through 1985–2014; 135 windows in the historical period). A 30-year period was adopted, aligning with the standard for climatological normals defined by the World Meteorological Organization (WMO). NAO is typically identified as the first mode (Wang *et al.*, 2012). However, consistent with Halifa-Marín *et al.*'s (2025) conclusions, we examined whether it can also appear as the second or third mode. To address this, we associated the leading three modes computed in each 30-year window with their canonical computation over the full period (e.g., 1851–2014) using Pearson

TABLE 1 All available simulations for each CMIP6 dataset analyzed in this study. Some models provide realizations with different forcings (f) or physics parameterization (p).

Model	Reference	Historical	Hist-nat	Hist-GHG	Amip-hist	ssp245	ssp585
ACCESS-ESM1-5	Ziehn *et al.* (2020)	40	3	0	0	40	40
CNRM-CM6-1	Voldoire *et al.* (2019)	29	10	9	9	6	6
CNRM-CM6-1-HR	Voldoire *et al.* (2019)	1	0	0	0	1	1
CanESM5	Swart *et al.* (2019)	65	50	50	50	50	50
CanESM5-1	Sigmond *et al.* (2023)	72	0	0	0	20	20
EC-Earth3	Döscher *et al.* (2022)	23	0	0	0	17	7
GISS-E2-1-G	Miller *et al.* (2021)	40	20	10	10	23	15
IPSL-CM6A-LR	Boucher *et al.* (2020)	33	10	10	10	11	7
MIROC-ES2L	Hajima *et al.* (2020)	30	0	0	0	30	10
MIROC6	Tatebe *et al.* (2019)	50	50	50	50	50	50
MPI-ESM1-2-LR	Müller *et al.* (2018)	50	30	30	30	30	50
MPI-ESM1-2-HR	Mauritsen *et al.* (2019)	10	0	0	0	2	1
UKESM1-0-LL	Sellar *et al.* (2020)	19	0	0	0	5	5

correlation of their spatial patterns (step 2 in Figure 1). In climate models, the NAO's identification during the running 30-year windows was similarly based on its canonical pattern in 20CRv3. This approach ensures that all NAO spatial patterns are identified using consistent reference characteristics, avoiding intermodel or intersimulation differences.

2.2.3 | Disentangling the variations of the NAO pattern

The comparison of the NAO spatial pattern across datasets and time periods was based on the movement of its action centres, identified by the location of the highest and lowest values in the EOF loadings as Halifa-Marín *et al.* (2025) described. For that purpose, two metrics are evaluated. The gradient (g) is quantified by the dimensionless range between the NAO centres in relation to their distance, which is computed by the Haversine formula (step 3 in Figure 1; Equations S5–S7). Additionally, the flux direction (fd, expressed in degrees) was determined by the arc/inverse tangent of the distance between centres (Δlon and Δlat, see Equations S8 and S9), converting the units from radians to degrees ($180/\pi + 180°$), and adding 90° to capture the origin of fd, which is perpendicular to the gradient line connecting the action centres (Equation S10, step 3 in Figure 1). We obtained a single value of g and fd for each period (step 3, Figure 1). Although we detected the centres of action in the EOF field, whose values may not be physically representative, Halifa-Marín *et al.* (2025) proved that those locations resemble where NAO/PC1 captures more SLP variability.

The variables g and fd were clustered using the k-means algorithm to differentiate NAO patterns in the 20CRv3 and CMIP5/CMIP6 datasets. Both series were normalized to a range of 0–1 by subtracting their minimum value and dividing by their range (Figure 2b, Equations S11 and S12). For climate models, normalization was based on the value ranges observed in the 20CRv3, meaning g and fd may exceed the 0–1 range. Also, clustering in CMIP5/CMIP6 datasets used the centroids derived from 20CRv3, ensuring that all simulated NAO patterns were classified to observed NAO patterns in 20CRv3.

2.2.4 | Precipitation changes driven by NAO pattern shifts

The relationship between NAO pattern and precipitation, with a focus on Europe, was analyzed across different NAO clusters. These analyses used the canonical NAO index calculated over the entire period provided by each dataset. Correlations between precipitation and NAO index were quantified using Pearson's method and assessed for significance ($p \leq 0.05$) with a t-test. Cluster-specific correlation composites represent the average correlation in their 30-year windows and were deemed significant if observed in at least 90% of those periods.

Relative winter precipitation changes were calculated as anomalies normalized by the average (Equation S13). The significance of precipitation changes was evaluated

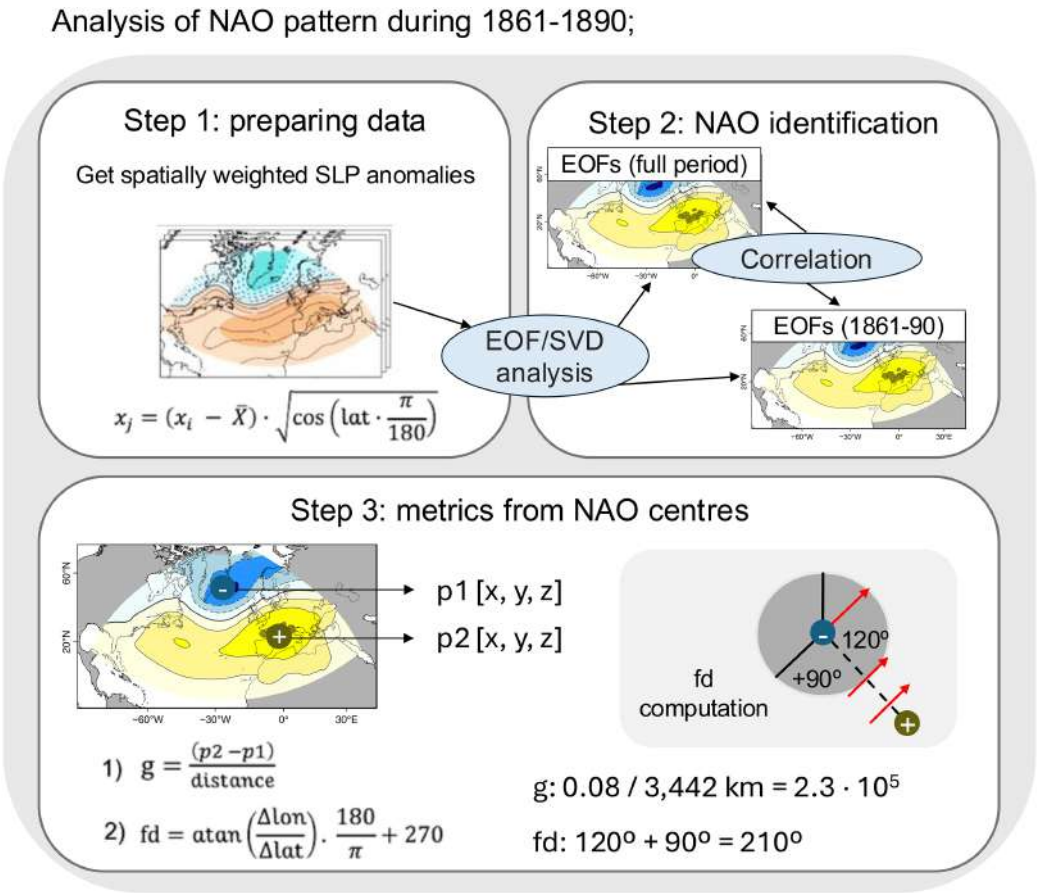

FIGURE 1 Graphical abstract showing the procedures to obtain the metrics of gradient (*g*) and coming-from flux direction (fd), exemplified by the 30-year window from 1861 to 1890. Step 1 prepares the matrix of spatially weighted anomalies of winter sea level pressure (SLP). Step 2 computes the empirical orthogonal modes (EOFs) 1–3 for the complete period (canonical characteristics, e.g., 1851–2014) and for 1861–1890. Those groups of EOFs are associated by highest correlation of their spatial pattern (EOF fields). Once we have identified the North Atlantic Oscillation (NAO) pattern during all periods, Step 3 obtains the metrics *g* and fd based on the two action centres defined in 1861–1890. Red arrows illustrate the flux direction in the panel of fd computation. [Colour figure can be viewed at wileyonlinelibrary.com]

using the Mann–Whitney test, comparing NAO+ (above the 70th percentile) and NAO− (below the 30th percentile) phases between each cluster and the full period. Trends and their significance in precipitation changes were quantified using Sen's slope method and the Mann–Kendall test.

2.2.5 | Observed-like long-term NAO variability in climate models

This analysis aims to determine whether, given the same NAO pattern, the implications for its teleconnection with European precipitation are consistent across reanalyses and climate models. The method identifies 30-year periods in simulations that yield the same *g* and fd values for each period in 20CRv3, considered its analogue (Figure S1). Additionally, the coordinates of both action centres must fall within their range observed for each cluster in 20CRv3, as well as the intensity of the centres (loadings in the EOF spatial pattern). These criteria ensure that similar *g* and fd values are not due to differing positions of the action centres but rather that the simulated NAO pattern accurately reflects the observed one (Figure S1). The position of the action centres is a crucial step, as the initial hypothesis suggests that their variability influences changes in the direction of the westerlies, thereby modifying NAO's impact on precipitation regimes, as also proposed in the literature (Hu *et al.*, 2022).

Consequently, this 'idealized' simulation includes the same number of clusters as those identified in 20CRv3, with each cluster containing no more than the corresponding number of periods observed in 20CRv3. Once a period with an analogue NAO is assigned to the idealized simulation, it is removed from the pool of potential candidates for subsequent target periods to ensure it is not reused. Selecting the same number of periods as observed in 20CRv3 clusters, even for future scenarios with

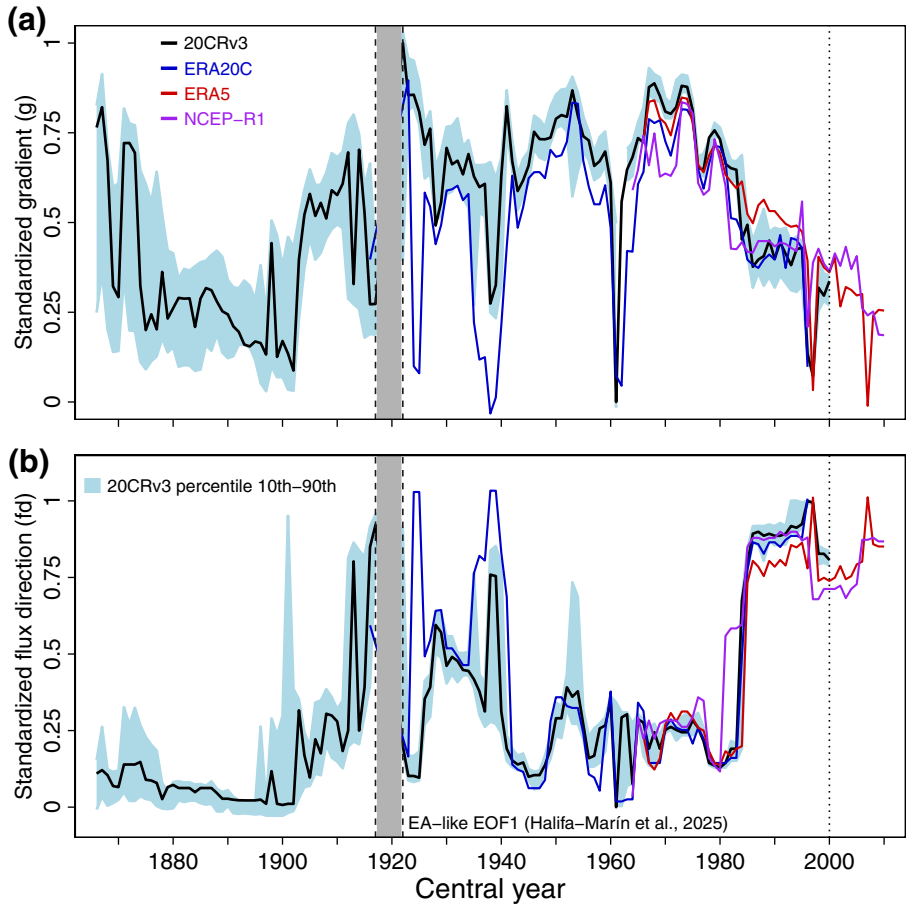

FIGURE 2 (a) The standardised gradient (*g*) observed in the 30-year windows of the 20CRv3 80-member ensemble (black line), ERA5 (red), ERA20C (blue) and NCEP reanalysis (purple). The light blue shading represents the range between the 10th and 90th percentiles identified across the 80 members of the 20CRv3 dataset. (b) The same for the flux direction (fd) metric. The windows from 1903–1932 to 1906–1935 were excluded based on the findings of Halifa-Marín *et al.* (2025), who identified an East Atlantic (EA)-like empirical orthogonal mode 1 (EOF1) during these periods. The dashed line marks the end of the study period analyzed, although ERA5 and NCEP extend the data up to 2024. [Colour figure can be viewed at wileyonlinelibrary.com]

fewer available years, is applied to maintain comparable statistics.

3 | RESULTS

3.1 | Types of NAO pattern observed in the Industrial Era

Three NAO patterns were identified using *k*-means clustering in the 80-member ensemble of 20CRv3 (Figures 2–5). A total of 33 periods (24%) were classified in Cluster 1 (NAO-C1), spanning the late 19th to early 20th century (Figure 5a). NAO-C1 is characterized by SW–W fd (mean 207°, ranging from 201° to 243°, Figure 3c), and a weak *g* (Figure 2a). The northern action centre is located between Iceland and Greenland (typical for the canonical NAO pattern), while the southern centre shifts unusually to northern Italy. NAO-C1 explains an average of 44% of variance (ranging from 36% to 48%). The NAO-C2 includes 74 periods (55%), primarily detected from the 20th century before the 1970s. The pattern aligns with canonical NAO descriptions, with northern and southern centres located between Iceland–Greenland and the Azores–Iberian Peninsula, respectively. It features a *W* flux direction (mean 231°, ranging from 209° to 274°) and canonical-like *g* values. NAO-C2 explains an average of 41% of the variance (ranging from 34% to 55%). NAO-C3 includes 24 periods (18%), mainly found from 1969 to 1984 onwards. NAO-C3 is characterized by a NW fd (mean 311°, ranging from 287° to 328°) and a weakened *g*. The northern centre shifts eastward (unusual), while the southern centre remains over the Azores (typical). NAO-C3 explains higher variance, averaging 50% (ranging from 32% to 56%). Additionally, 30-year periods from 1903–1932 to 1906–1935 (3%) in which the EOF1 reflects an EA pattern were excluded from the clustering (referred to as the 'Out' group).

These patterns feature a northern centre over Svalbard (similar to NAO-C3) and a southern centre resembling the broader EA centre, as described by Halifa-Marín *et al.* (2025). This multidecadal variability of the NAO has been analyzed across periods covered by ERA-20C, ERA5, NCEP-R1, and the ensemble of individual members from 20CRv3 (Figure 2). Although the greatest uncertainties are associated with periods where only 20CRv3 extends (second half of the 19th century), ERA-20C successfully reproduces the four clusters identified in 20CRv3 (Figure S2).

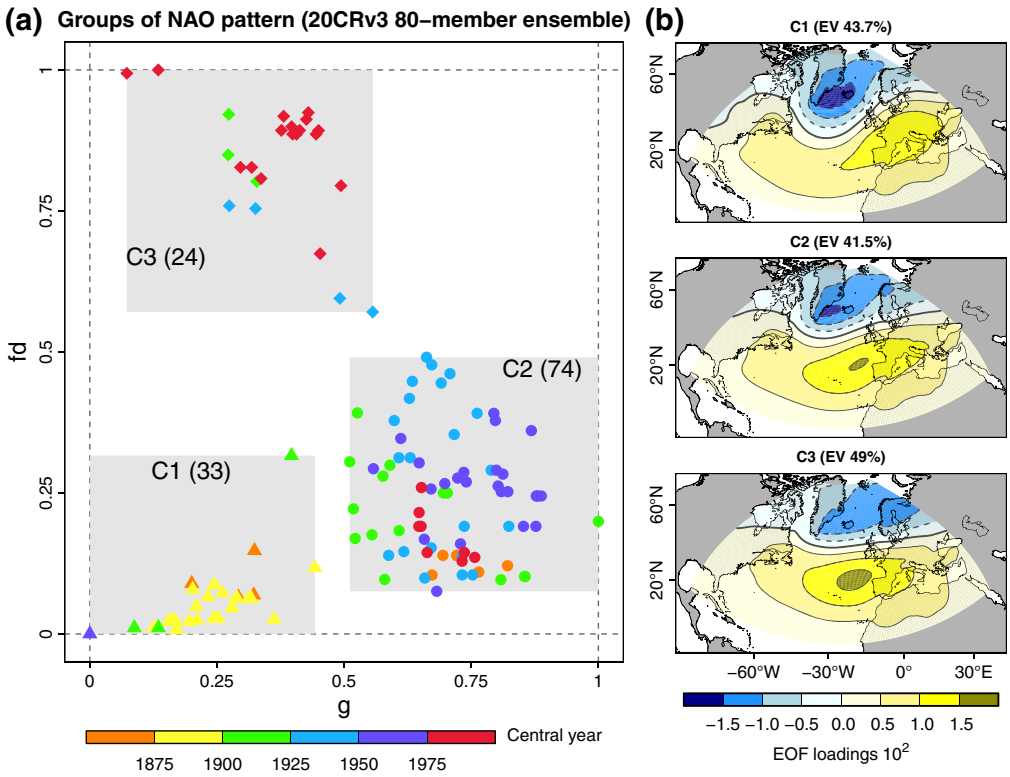

FIGURE 3 (a) Clustering by *k*-means algorithm for normalized gradient (*g*, x-axis) and flux direction (fd, y-axis). The triangles (C1), circles (C2), and diamonds (C3) identify those variables for each 30-year period. Colour of the symbols represents the central year of the periods by intervals of 25 years from 1850 to 2000. The limits for each cluster in the *g*–fd space is marked with grey squares. Number of periods clustered in each group is noted in parentheses. (b) The mean EOF loadings pattern for periods grouped in each cluster (rows), indicating the averaged explained variance (EV) in the title. [Colour figure can be viewed at wileyonlinelibrary.com]

Meanwhile, ERA5 (Figure S3) and NCEP-R1 (Figure S4) consistently detect the emergence of NAO-C3 from the late 20th century onward. The 'Out' cluster is identified in ERA-20C during the same periods as in 20CRv3, a result previously noted in Halifa-Marín *et al.* (2025). Given these findings, this study focuses on the 20CRv3 ensemble, assuming it represents the most reliable source for understanding NAO variability during the Industrial Era.

3.2 | Observed NAO–precipitation links among clusters

In NAO-C1, two regions with strong negative correlations (below −0.8) were observed in the Iberian and Balkan Peninsula (Figure 4a). In NAO-C2, negative correlation generally weakened, except over the Iberian Peninsula. In NAO-C3, negative correlations further diminished in the Balkan Peninsula, while showing slight intensification in the Iberian Peninsula. Positive correlations were higher (above 0.85) over Iceland by NAO-C1 but progressively weakened for subsequent clusters. In contrast, positive correlation strengthened from NAO-C1 to NAO-C3 in northern Europe (e.g., Scandinavia). A notable shift in central Europe (e.g., Germany) was observed, where negative correlations in NAO-C1 transitioned to positive correlations in later clusters, particularly NAO-C3. These findings indicate significant changes in NAO-driven precipitation patterns across clusters (Figure 4b), consistent with analyses from an observation network in southern and central Europe (Figure S5).

Four European regions emerge as key areas of interest: the western Iberian Peninsula (12° W–2° E, 35–43° N) and Scotland (9–4° W, 55–60° N), due to their strong NAO influence and evident multidecadal variability in precipitation modulation, as well as central Europe (5–15° E, 49–55° N) and the Balkan Peninsula (16–24° E, 42–46° N), where substantial intensification or weakening of NAO–precipitation correlations was observed among clusters (Figures 5a and S5a).

Other regions may also be relevant (e.g., eastern Canada, northern Europe) but were not covered by the observation network used. It is noteworthy that NAO-C1 (late 19th to early 20th century) and NAO-C2 (mid-20th century) coincided with dominant NAO− conditions, whereas NAO-C3 aligns with dominant NAO+ phases

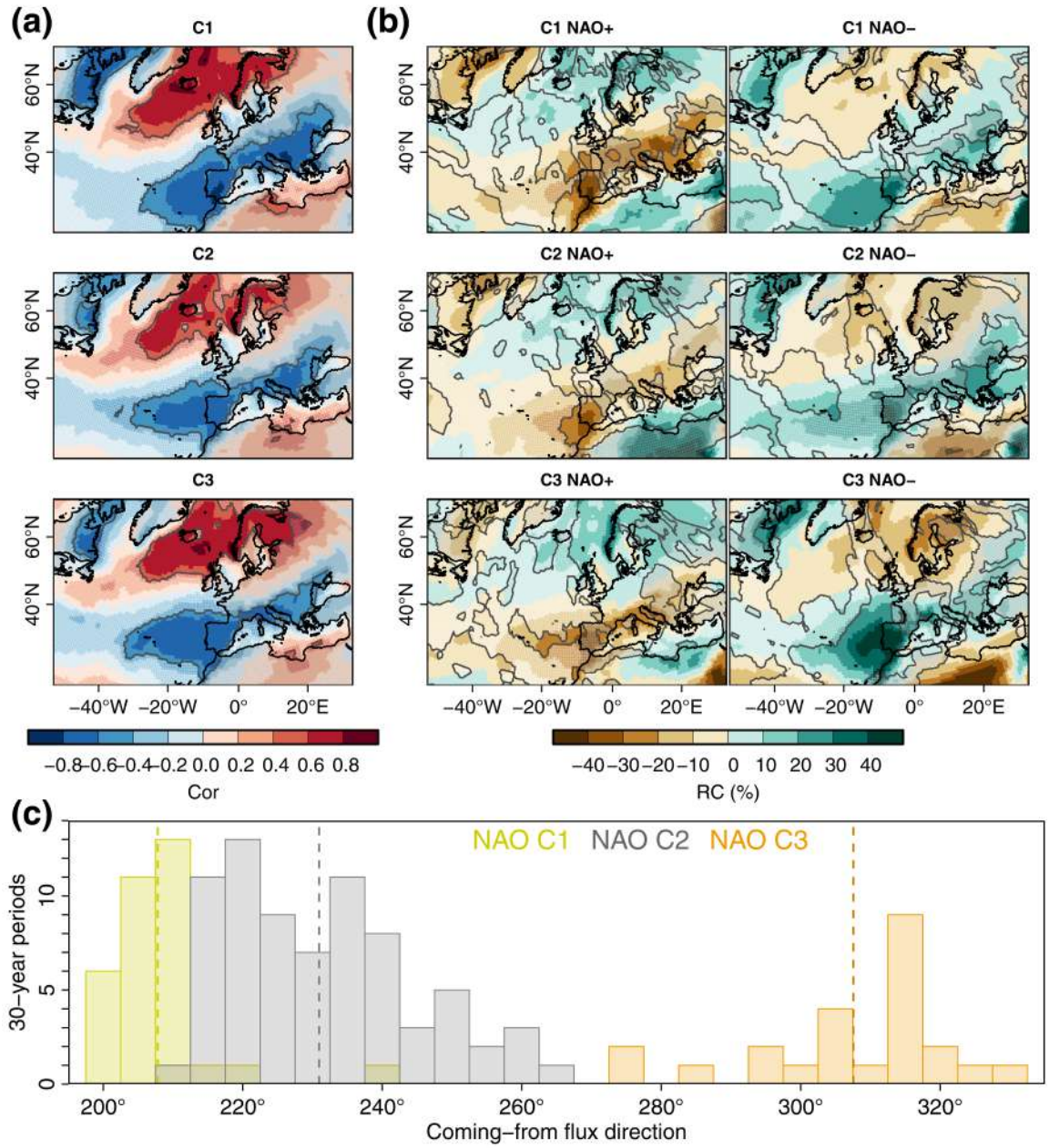

FIGURE 4 For each cluster identified in Figure 3, panel (a) shows the average correlation between NAO index (30-year averaged from NAO index computed in the full period) and winter precipitation. (b) The mean relative change (RC) of WP under NAO+ and NAO− phases (related to their magnitude in the full period 1851–2014). Significant estimates are strongly coloured and highlighted with contours. (c) Histogram (absolute frequency) of fd detections in each cluster (yellow = C1, grey = C2, orange = C3), identified by *k*-means clustering. Dashed lines note the mean fd for each group. [Colour figure can be viewed at wileyonlinelibrary.com]

(Figure 5a). Observations recorded very wet conditions in the Balkan Peninsula during NAO-C1 (Figure 5b), while near-neutral precipitation changes were observed in NAO-C2, despite sharing NAO− dominance. This disparity may reflect the expansion of the North Atlantic subtropical ridge toward the western Mediterranean and Central Europe during NAO+ in NAO-C1 (Figure 3b), compared to the deepening of low-pressure systems promoting moist winds toward the western Balkan coast (Figures 3 and 4). However, NAO-C2 shows increased precipitation in this region in the 20CRv3 (Figure 5c), likely due to differences in data sources, as this dataset includes interior areas of the peninsula beyond the two rain gauges analyzed.

Similarly, central Europe experienced significant precipitation decreases during NAO-C1, weak increases during NAO-C2, and significant increases during NAO-C3, driven by a NAO+ phase (Figures 4, 5 and S2). This transition corresponds with a prevailing NW fd in NAO-C3

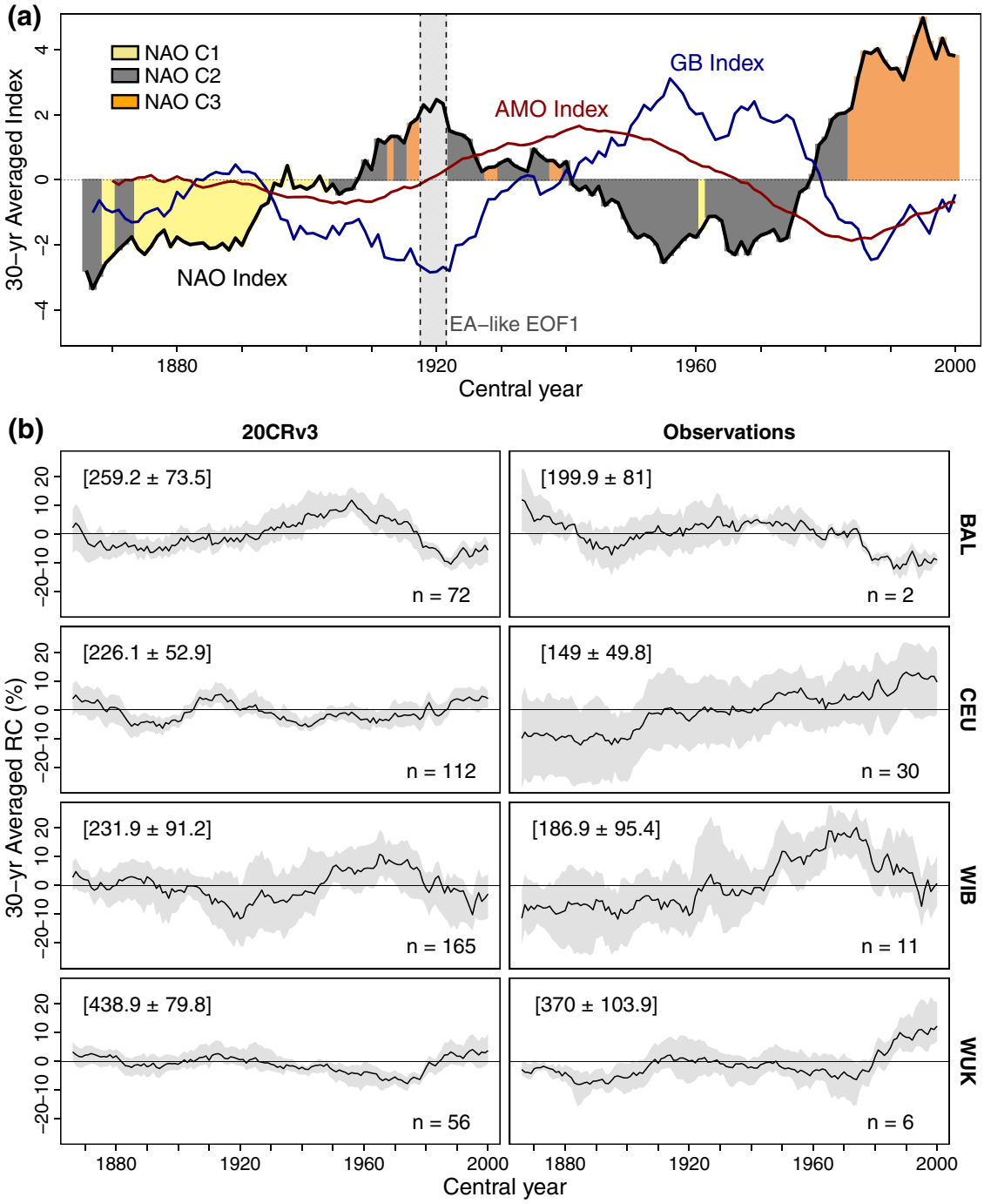

FIGURE 5 (a) The 30-year averaged moving NAO index (black line) from PC1 computed in the full period of 20CRv3 (1851–2014). Greenland Blocking (blue line, GB) and Atlantic Multidecadal Oscillation (red, AMO) are also displayed. (b) The 30-year averaged RC of winter precipitation seen in the 20CRv3 and observations (black lines) for selected European regions: Western Balkan Peninsula (BAL, framed in 16–24° E, 42–46° N); central Europe (CEU, 5–15° E, 49–55° N); western Iberian Peninsula (WIB, 12° W–2° E, 35–43° N); and western United Kingdom (WUK, 9–4° W, 55–60° N). The grey-shaded area denotes the range of the RC obtained within all grids (20CRv3) or rain gauges (observations). The number of grids/gauges is noted in the plots. Plots in (b) clarify the average precipitation and standard deviation by region. [Colour figure can be viewed at wileyonlinelibrary.com]

(Figure 3b), driven by the northward expansion of the Azores High. Similarly, this aligns with the presence of Scandinavian Blocking (SB), coupled with GB affecting Northern Europe during NAO− (Figure 3b). The recent rise in winter precipitation over this region, captured more strongly by rain gauges, contrasts with the wet periods recorded during NAO-C1 in 20CRv3 (Figure 5c).

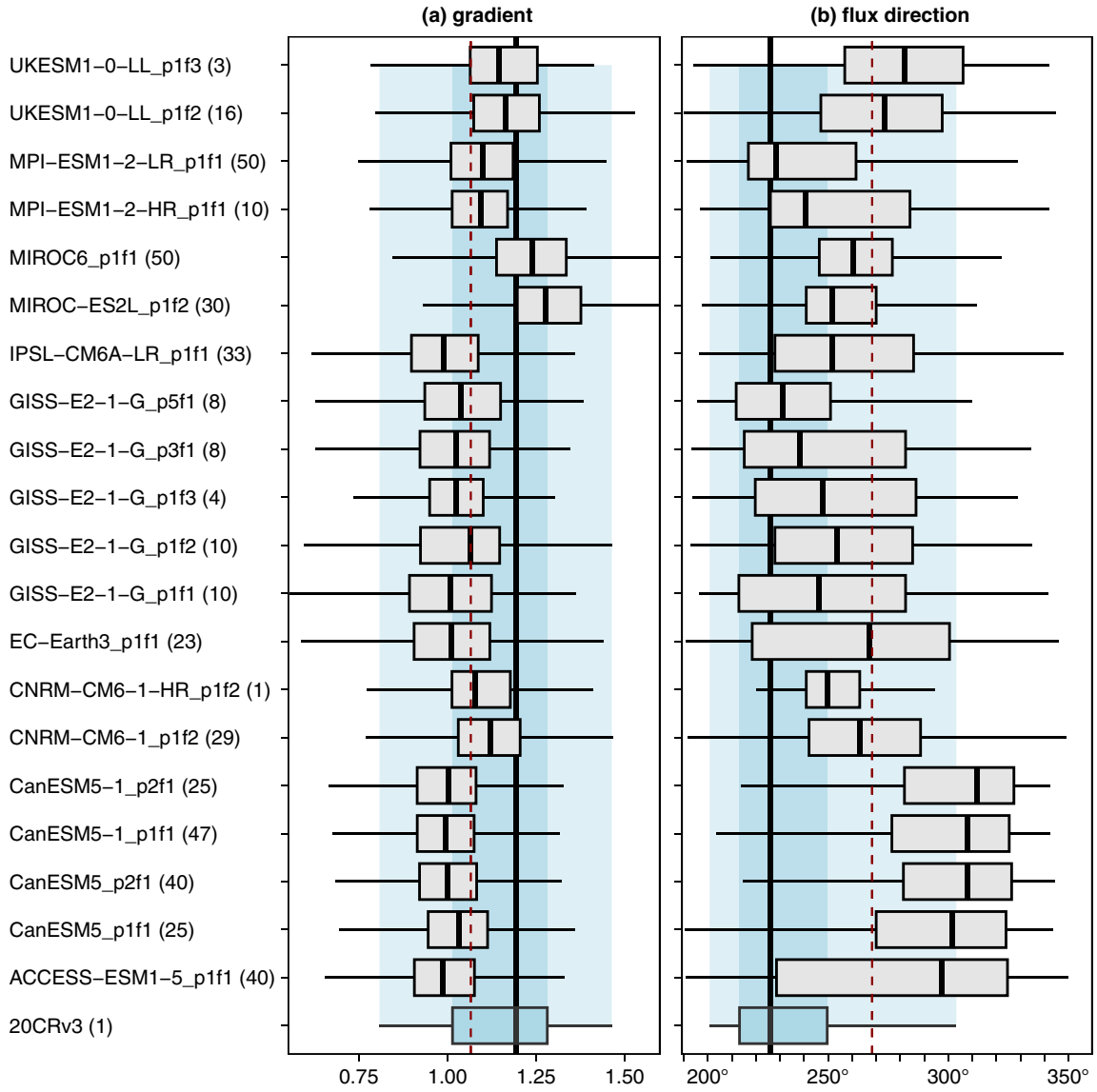

FIGURE 6 Box plot (x-axis) of the gradient (g [a], whose units are defined in Section 2.2.3) and flux direction (fd [b], in degrees) for all analyzed historical simulations (462) grouped by model (11 models, y-axis) and the 20CRv3 reanalysis (at the bottom). The box for the reanalysis is coloured in light blue, and the boxes for the models are in grey. The 5th to 95th percentage range (very light blue area) and the 25th to 75th percentage range limits (light blue area) in 20CRv3 are illustrated. In addition, a solid black line marks the median in 20CRv3, and a dashed red line marks the median for simulations. Outliers are not presented for boxes. [Colour figure can be viewed at wileyonlinelibrary.com]

The western Iberian Peninsula and Scotland displayed consistent NAO modulation across all clusters, though more pronounced in NAO-C3 (Figure 4a). During NAO-C3, more NAO+ activity and a broader southern action centre in the EOF field (Figure 3b) indicate more frequent Azores Highs (NAO+), resulting in wetter winters in the UK and drier conditions in the Iberian Peninsula. Conversely, NAO− phases bring more intense low-pressure systems to the Iberian Peninsula (Figure 4b).

Overall, the temporal sequence of clusters identified in 20CRv3 (our chronology for multidecadal changes in NAO) appears to be linked to the intensity of GB and the AMO sea surface temperature variability (Figure 5). NAO-C3 aligns with a period of high GB intensity, which itself is associated with a positive AMO phase. Differences in GB intensity during the two NAO− periods (NAO-C1 and NAO-C2) may explain the distinctions between its spatial pattern in these clusters. The stronger AMO− phases observed since the late 20th century could account for the persistence of NAO-C3, which contrasts with the less robust NAO+ dominance during the early 20th century.

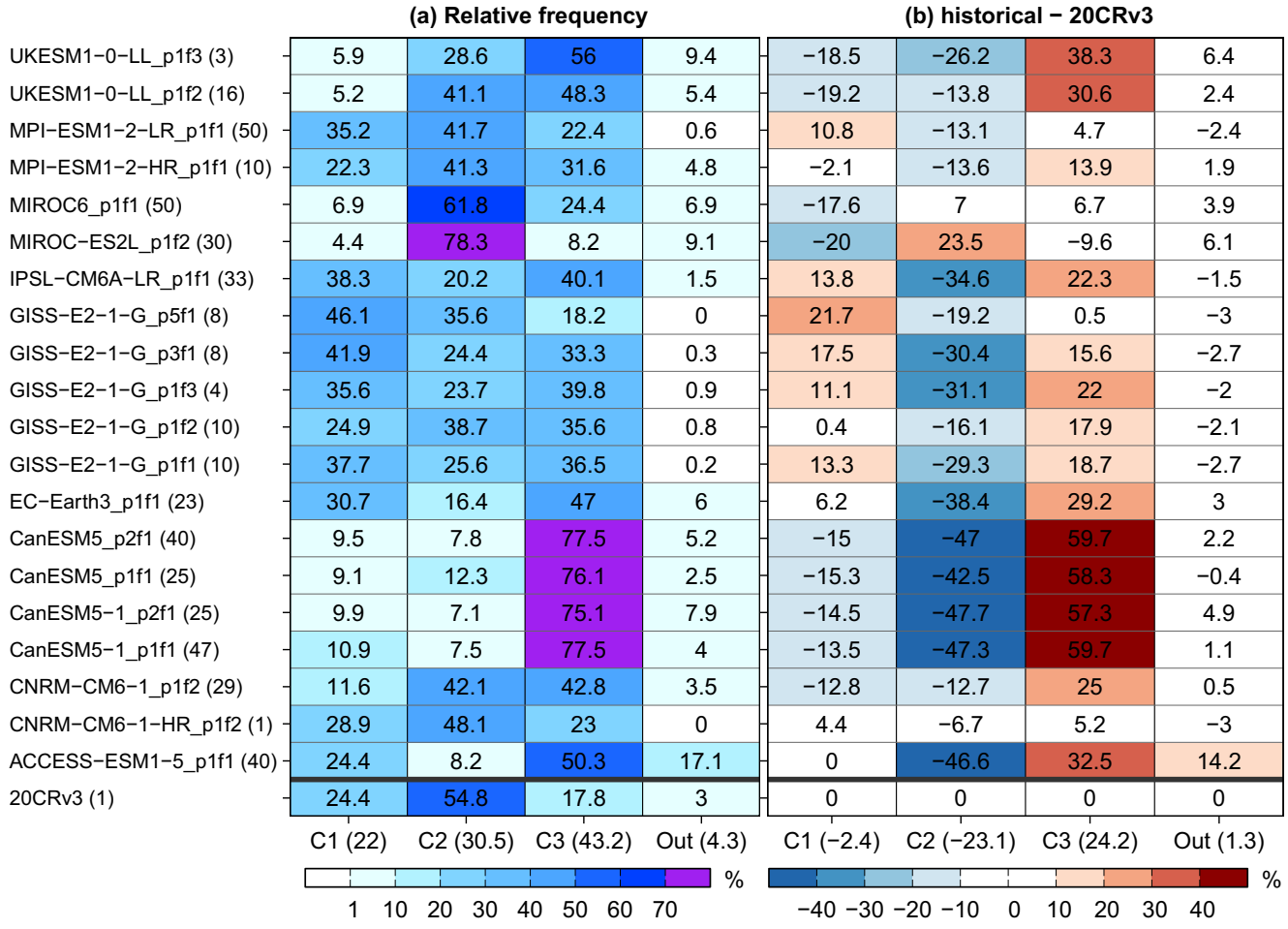

FIGURE 7 (a) Relative frequency of 30-year periods classified by NAO clusters in the historical simulations and the 20CRv3 reanalysis (y-axis). The number of simulations is indicated in the y-axis labels. The labels for the x-axis indicate the average by clusters. (b) Similar to (a), the absolute difference between the relative frequency of clusters in relation with 20CRv3. [Colour figure can be viewed at wileyonlinelibrary.com]

3.3 | Skill of climate simulations capturing the long-term variability of NAO

Most historical simulations exhibit g values within the observed range in 20CRv3, although their medians differ significantly (Figure 6a). Most models underestimate g, with the exception of MIROC simulations. Conversely, the overestimation of the fd is very noticeable, often showing interquartile ranges outside the limits of 20CRv3 (e.g., CanESM5, Figure 6b). The most frequent fd shifts from 227° (SW) to 269° (W), with CanESM5 displaying a distinct NW direction.

For both metrics, high-resolution simulations (MPI-ESM1-2-HR and CNRM-CM6-1-HR) do not show improved performance compared to their coarser-resolution counterparts. Similarly, we found no improvement between CanESM5 and its upgraded version CanESM5-1. We also found no differences between their simulations with different physics parameterization p1 or p2 (e.g., CanESM5), nor between UKESM-1-0-LL simulations with different forcing (f2 or f3). Only GISS-E2-1-G seems to be sensitive to changes in physics and forcing, capturing fd as observed.

That poor reproduction of g and, particularly, fd by historical runs leads to noticeable differences in NAO clustering (Figure 7). Overall, the simulations underestimate the frequency of NAO-C2 periods (−23% compared to 20CRv3, Figure 7b), while the frequency of NAO-C3 is largely overestimated (+24%), and NAO-C1 also slightly underestimated (−2%). For instance, CanESM5 and CanESM5-1 simulations (with runs using different parameterization of physics) overestimate NAO-C3 above 57%. MPI-ESM1-2-LR shows the best fit capturing the frequencies of the clusters observed in 20CRv3. The CNRM-CM6-1-HR simulation does improve significantly the results of its low-resolution simulations, but one simulation is assessed, so it does not allow comparable statistics. To ensure a proper comparison with

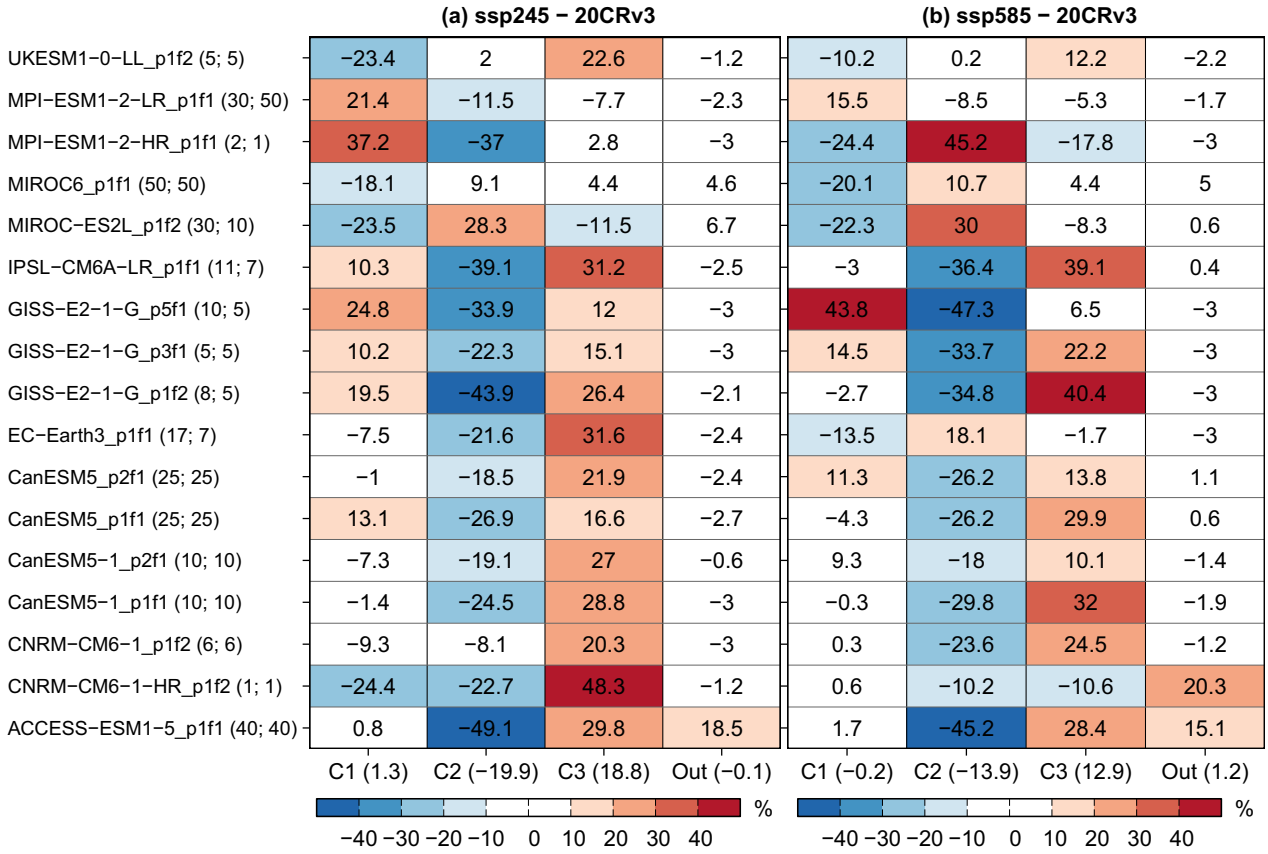

FIGURE 8 Similar to Figure 7b, for 287 runs and 262 runs of experiment ssp245 and ssp585, respectively, by 11 models. Y-axis labels indicate the number of runs by model used in both datasets. [Colour figure can be viewed at wileyonlinelibrary.com]

20CRv3 clustering, the 'Out' group (EOF1 resembling an EA-like pattern) was also analyzed in historical runs. Two models failed to reproduce those periods, though ACCESS-ESM1-5 substantially overestimated (+17%). On average, no significant bias was detected for this cluster (−0.2%). It is important to clarify that the 'Out' cluster in the models represents those NAO patterns that are not the EOF1. These patterns may exhibit EA-like structures (as we noted in 20CRv3) or others, which are not analyzed in this study.

These findings suggest that a zonal arrangement of both action centres (NAO-C2 pattern) is less frequently reproduced in climate simulations, while NAO-C3 (mostly observed in recent periods) appears more often.

The biases found in historical simulations for *g* and fd are also evident in hist-nat, hist-GHG, amip-hist and piControl simulations. In hist-nat runs (Figure S6), NAO-C1 is slightly overestimated (1%), NAO-C2 is significantly underestimated (−25%), and NAO-C3 overestimated (+23%). The 'Out' cluster is slightly overestimated (Figure S6). Similarly, hist-GHG outputs (Figure S7) underestimate NAO-C1 (−1%), NAO-C2 is severely underestimated (−20%), and NAO-C3 overestimated (+21%). The 'Out' cluster is underestimated by −0.5%.

The skill improves in amip-hist simulations (Figure S8), where NAO-C1 (−6%) and NAO-C2 (−15%) is underestimated, and NAO-C3 is overestimated (+22%). The 'Out' cluster does not vary related to 20CRv3(−1%). Lastly, piControl simulations exhibit biases similar to historical simulations (Figure S9): NAO-C1 is underestimated on average (−3%), NAO-C2 is generally underestimated (−26%), and NAO-C3 is overestimated (27%).

The results reveal two contradictory signals. On the one hand, the nature of the forcing appears to have limited impacts on improving the model's ability to accurately capture the three observed NAO patterns. When comparing the estimates of NAO clusters across attribution simulations, no significant differences emerge between applying only natural forcing or only anthropogenic forcing. On the contrary, the historical, hist-nat, and hist-GHG simulations display biases in the NAO clusters similar to those observed in the piControl simulations. Interestingly, in those simulations without any forcing, the bias relative to 20CRv3 is even greater, although this should be interpreted with caution due to the smaller number of realizations.

On the other hand, under the higher-emissions scenario (ssp585), the frequency of NAO clusters aligns more closely with 20CRv3 (Figure 8). Biases in the ssp585

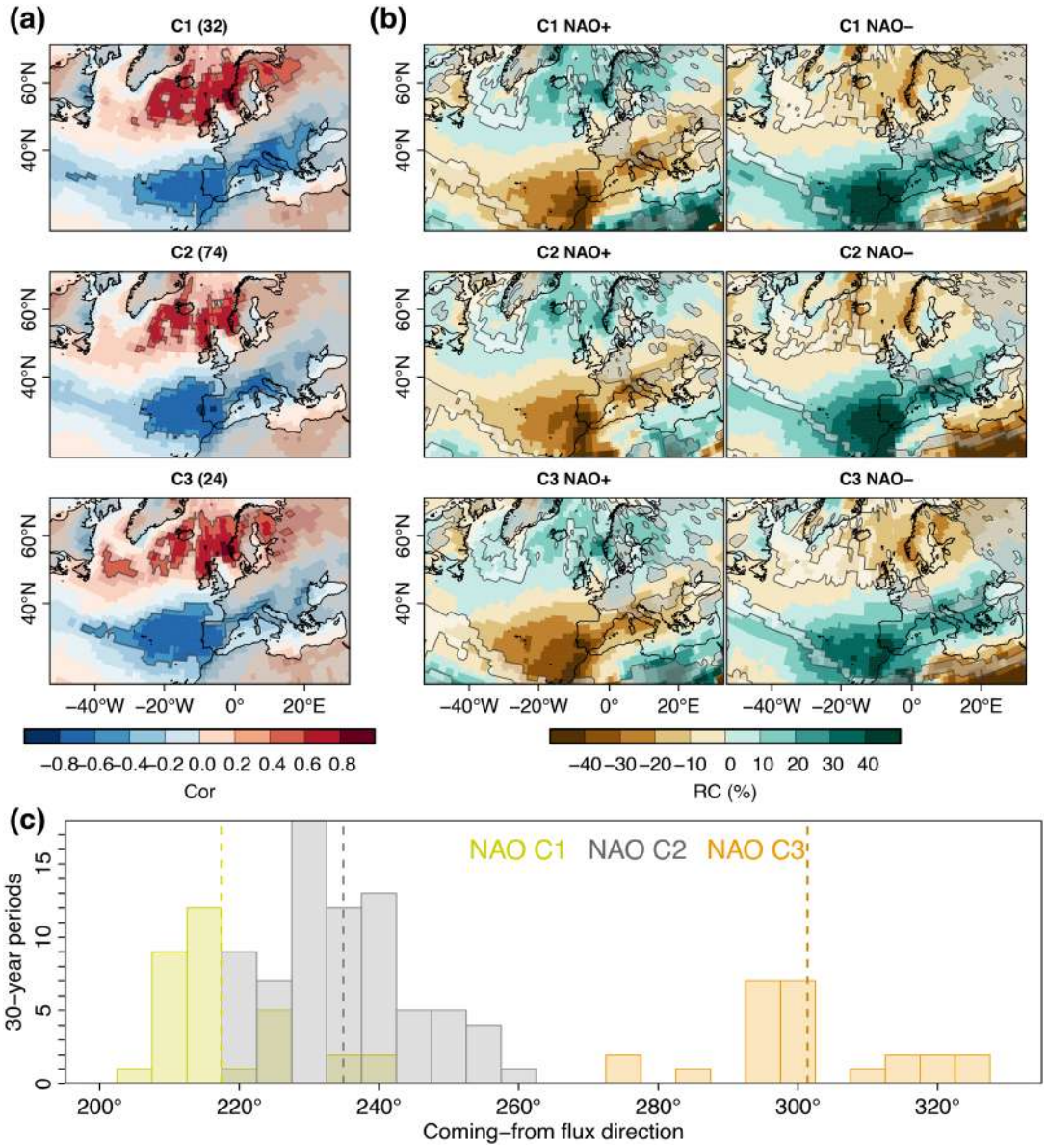

FIGURE 9 Similar to Figure 4 but for an 'idealized' simulation detected in MPI-ESM1-2-LR simulations under ssp585 experiment (50 runs). The number of analogous periods identified within each cluster is indicated in the titles of (a). [Colour figure can be viewed at wileyonlinelibrary.com]

simulations displayed are reduced for NAO-C2 (−14%) and NAO-C3 (+13%), while NAO-C1 (−0.2%) and Out (+1%) show similar biases to historical runs.

These findings indicate a more zonal NAO performance in future scenarios, bringing NAO-C2 occurrence closer to its observed relative frequency in 20CRv3. Nevertheless, the overestimation of NAO-C3 persists in the future scenario.

Consistently, ssp245 experiments exhibit greater biases relative to 20CRv3 (Figure 8). In this dataset, the overestimation of NAO-C3 reaches +19%, while the underestimation of NAO-C2 is −20%. Focusing on MPI-ESM1-2-LR, whose historical simulations show the lowest total absolute bias, a notable decline is also observed applying higher levels of future forcings. CanESM5, another model with numerous realizations in historical and ssp245/585, shows smaller differences between future scenarios, although in both cases, the excessive bias in NAO-C3 seen in historical runs is significantly reduced.

Finally, analyzing CMIP5 historical simulations (Figure S10), the same general pattern of overestimated NAO-C3 observed in CMIP6 models is shown (+32%), although the historical CMIP6 simulations significantly reduce this overestimation. In historical CMIP5 simulations, the larger bias in NAO-C3 relative to 20CRv3

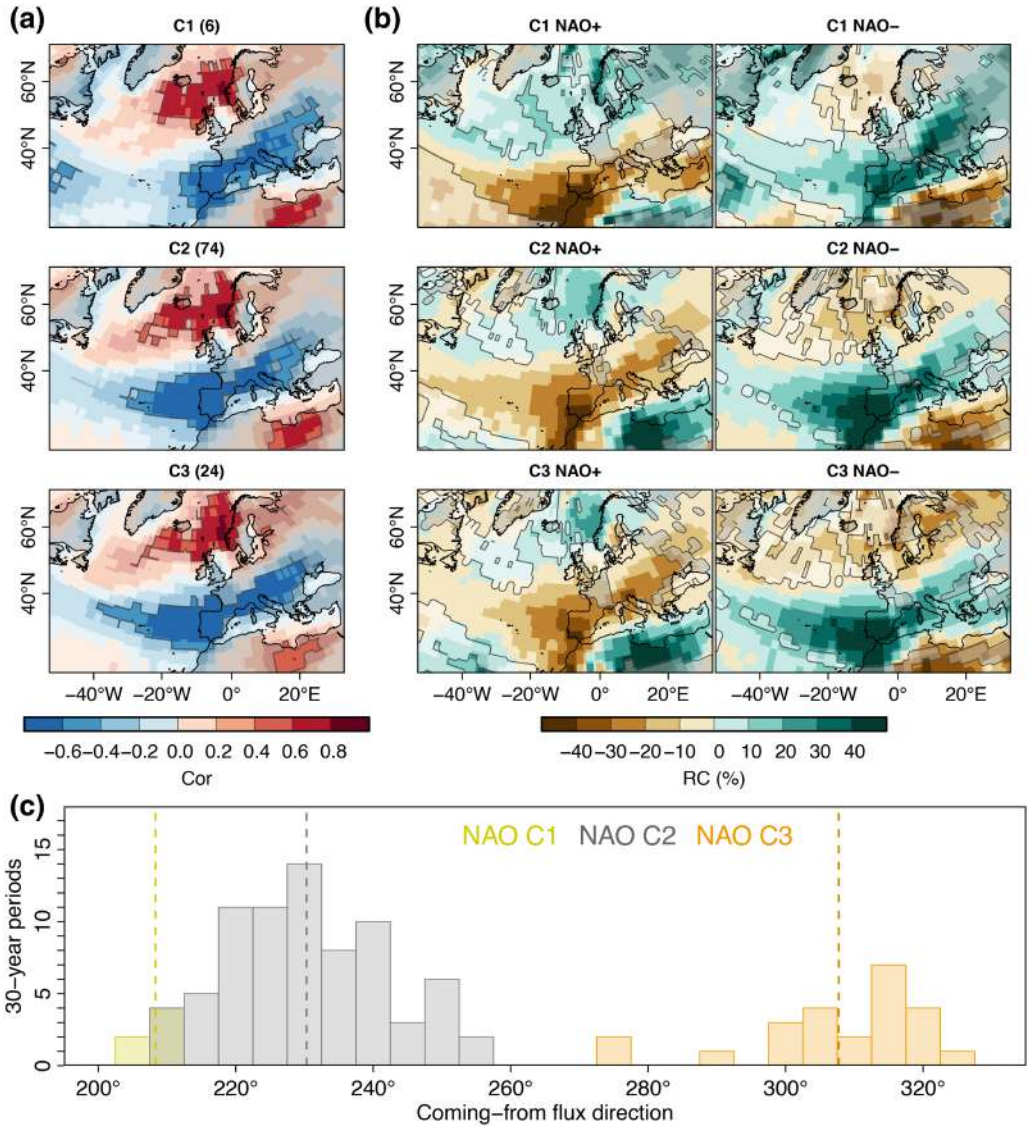

FIGURE 10 Similar to Figure 9 but for CanESM5 simulations. [Colour figure can be viewed at wileyonlinelibrary.com]

is balanced by a greater underestimation of NAO-C1 compared to the homologous CMIP6 simulations.

3.4 | Misinterpreted NAO variability amplifies uncertainties in projected precipitation

Following the procedures described in Section 2.2.5, we searched for periods analogous to those observed in 20CRv3 across two extensive simulation sets (50 members each) for the ssp585 experiment, provided by the MPI-ESM1-2-LR and CanESM5 models. This resulted in two sets of future NAO patterns replicating the NAO clusters from 20CRv3. For MPI-ESM1-2-LR, 130 periods were identified (Figure S11), with all observed periods finding an analogous NAO pattern except for one NAO-C1 window. Interestingly, Figure 9a shows that the correlation patterns between the NAO index and precipitation vary among clusters similarly to what is observed in 20CRv3. Specifically, the pattern of negative correlations shifts and intensifies towards the western Mediterranean and the subtropical North Atlantic, losing influence in the Balkan Peninsula in NAO-C3. Similarly, positive correlations intensify in NAO-C3 over northern Europe.

These findings demonstrate that once the NAO patterns and their multidecadal variability (as observed in 20CRv3) are reproduced, the influence of this mode of variability on Europe changes. In the case of CanESM5 (Figure 10a), finding analogous periods for NAO-C1 was more challenging, with only six windows identified (Figure S12). Nevertheless, the NAO–precipitation correlation pattern again shows a westward shift as the analysis transitions from NAO-C1 to NAO-C3. However, in this

case, the NAO does not lose influence over the Balkan Peninsula. The analysis of relative precipitation changes under different NAO phases across clusters also reveals significant differences, albeit with more noise. These variations underscore the distinct impact of the NAO on regional precipitation, reinforcing the notion that its multidecadal variability also influences precipitation variability in climate models. Additionally, both sets of analogue periods are able to associate flow directions of the same magnitude as those observed in 20CRv3.

4 | DISCUSSION

4.1 | Atmosphere–ocean feedback promoting the long-term variability of NAO

The observed long-term variability of the NAO has been thoroughly addressed in this study, highlighting several key aspects. First, the analysis identifies three distinct NAO patterns that exhibit a coherent spatial and temporal evolution. These patterns reveal pendular (W–E) displacements of the action centres, constrained between Iceland and Scandinavia (northern centre) and the Azores and Italy (southern centre). This clustering enables a detailed analysis of the frequency of each NAO pattern and illustrates abrupt shifts in the location of both action centres across different periods. This represents a significant improvement over earlier studies, which often focused on specific intervals (Halifa-Marín *et al.*, 2025; Moore *et al.*, 2013), or solely analyzed the uniqueness of the post-1980s shift (Wang *et al.*, 2012). It also complements findings from studies of the Common Era (Hernández *et al.*, 2020), the last millennium (Börgel *et al.*, 2020), and the Instrumental Period (Mellado-Cano *et al.*, 2019), which were based on sparser observational data.

Second, the modulation by NAO on the European climate is shown to differ significantly among the identified clusters. This extends the understanding of the non-stationary nature of NAO's influence on European climate previously described (Comas-Bru & McDermott, 2014; Vicente-Serrano & López-Moreno, 2008). This study links variations in mean flow direction (fd) to physically consistent changes in NAO-precipitation relationships across different European regions. For instance, during NAO-C3, the NW flow is blocked by the Alps, limiting the areas in Central Europe affected by NAO+ (Figure S5).

Additionally, these results support recent work by Hu *et al.* (2022), who attributed the loss of connection between precipitation proxies in northern Italy and NAO due to westerly splits affecting western Europe. Our findings demonstrate that similar mechanisms driving abrupt changes in precipitation records during the Middle Holocene can also be found in observations.

This study has not extensively explored the physical mechanisms underlying the multidecadal variability of the NAO. However, the analyses suggest that Atlantic SST variability may influence GB activity, potentially inducing shifts in NAO patterns (observed transitions between clusters). Figure 4 examines the multidecadal variability of the AMO and GB indices, revealing that GB weakens following an AMO+ phase, and vice versa, without establishing a clear causal relationship between the two phenomena. Periods of dominant NAO+ coincide with NAO-C3, although the intensification during the first half of the 20th century exhibits distinct characteristics (e.g., EOF1 resembling an EA-like pattern; Halifa-Marín *et al.*, 2025). Notably, NAO-C3 has dominated recent periods, a trend also observed in ERA5 (Figure S3). This coincides with a phase of strong AMO− but without the extreme weakening of GB observed in earlier phases. These findings suggest that the SST gradient in the Atlantic could play a primary role in the recent dynamic of the NAO, influencing GB variability. This hypothesis aligns with the observed interplay between SST anomalies, atmospheric blocking variability, and NAO pattern (Kwon *et al.*, 2020; Omrani *et al.*, 2022; Rimbu *et al.*, 2014; Woollings *et al.*, 2015), warranting further investigation into the underlying processes driving these interactions.

Numerous studies have emphasized the role of natural atmosphere–ocean interactions in driving changes for the NAO spatial pattern. Börgel *et al.* (2020) proposed that shifts in NAO action centres are linked to variations in North Atlantic SST, influenced by different phases of the AMO. Similarly, Hu *et al.* (2022) identified interactions between AMO and NAO, particularly through modifications in the SLP dipole over the Icelandic Low and Azores High.

Also, these interactions are present in the formation and persistence of atmospheric blockings. The literature has further explored the connections between the GB, the Atlantic Ridge (AR), and the SB variability, revealing alternating dominance of these phenomena over different periods (e.g., Rimbu *et al.*, 2014). Long-term SST variability, characterized by the AMO, has been proposed as a key driver for North Atlantic atmospheric blocking. This mechanism aligns with the ocean–atmosphere feedback described by Kwon *et al.* (2020). AMO itself is influenced by natural forcings such as solar cycles, volcanic activity (e.g., Birkel *et al.*, 2018; Knudsen *et al.*, 2014; Mann *et al.*, 2021), and interactions with the Atlantic Meridional Overturning Circulation (AMOC) (Börgel *et al.*, 2022; Kim *et al.*, 2021). These factors result in SST anomalies across diverse regions and timescales, transcending the commonly recognized north–south thermal gradient and the

60–70-year warm–cold oscillations of AMO phases (Birkel *et al.*, 2018).

This interplay contributes to the nonsimultaneous occurrence and persistence of GB, SB, and AR, potentially serving as a critical modulator of NAO fluctuations (Kwon *et al.*, 2020; Rimbu *et al.*, 2014). Despite the natural variability of AMO, evidence suggests anthropogenic radiative forcing has influenced North Atlantic SSTs, consistent with global ocean warming since the 1800s (McGregor *et al.*, 2015; Walker *et al.*, 2022). The observed North Atlantic warming during the Common Era contrasts with the recent cooling observed in the Subpolar Gyre (Oltmanns *et al.*, 2020; Singh *et al.*, 2018). This cooling, likely linked to Greenland ice melt, has been identified as a trigger for the absence of GB and the northward shift of winter storm tracks over northern Europe since the 1980s (Oltmanns *et al.*, 2020). However, it may also mask the impact of the increased thermal gradient between the Arctic and subtropical North Atlantic, as identified by Hu *et al.* (2022) in this context. Despite uncertainties in AMO–NAO relationships (Smith *et al.*, 2020), the ocean–atmosphere feedback and anthropogenic SST forcing can suggest that recent NAO behaviour is likely a combination of natural variability and signals of a warming climate. Furthermore, the ocean's response to global warming also remains debated. Some studies warn of drastic AMOC changes already underway (Ditlevsen & Ditlevsen, 2023), while others argue that the AMOC has shown no forced changes (Latif *et al.*, 2022).

Additionally, the NAO variability could also be driven by the thermodynamic strengthening of the Azores High (Cresswell-Clay *et al.*, 2022) and the expansion of the Hadley cell (Grise & Davis, 2020) due to warming in the northern tropics. However, this matter remains under debate, as recent studies notice that projections of Hadley cell expansion are not conclusive, particularly for the Northern Hemisphere (Lionello *et al.*, 2024; Wu *et al.*, 2024).

4.2 | Misinterpreted North Atlantic climate system by CMIP6 datasets

This study evaluates whether the observed long-term variability of NAO spatial patterns is adequately reproduced by CMIP6 models. While the gradient (g) is generally well captured – albeit slightly underestimated – this aligns with AR6-IPCC findings, which noted that the slight underestimation of SLP anomalies related to NAO action centres remains unresolved between CMIP5 and CMIP6 (Gulev *et al.*, 2021, and references therein). Conversely, the fd is significantly underestimated, a shortcoming unproven in IPCC AR6, which demonstrates the misrepresentation of action centre mobility in climate models. This limitation has critical implications for accurately simulating the climate system and is likely linked to persistent issues in reproducing long-term variability in the Polar Jet and blocking events, as noted in previous studies (Bracegirdle, 2022; Dorrington *et al.*, 2022; Schiemann *et al.*, 2020).

Our results indicate that, while the models can capture all the NAO clusters identified in 20CRv3, they poorly reproduce their frequency. NAO-C3 is notably overestimated across simulation sets. The positive bias is found in historical (Figure 7), hist-nat (Figure S6), and hist-GHG (Figure S7). In future scenarios, the overestimation of NAO-C3 persists but is reduced by half in SSP585 compared to the historical period (Figure 8). This overestimation also is not removed in amip-hist simulations (Figure S8), where SST is prescribed with HadISST dataset (Rayner *et al.*, 2003). The piControl simulations reveal similar bias for NAO-C3, even compared to runs with altered forcings (Figure S10). Furthermore, this overestimation was more pronounced in CMIP5 historical runs (Figure S9).

Given the recent observational prevalence of NAO-C3, this raises questions: are models tuned to recent atmospheric dynamics? Does excessive sensitivity to forcing in the simulations contribute to this bias? Or does this overestimation of NAO-C3 reflect a singular behaviour of the NAO driven by global warming? Christiansen *et al.* (2022) addressed similar questions, demonstrating that CMIP6 datasets perform better in reproducing observed NAO index variability post 1970. Specifically, the correlation between observed and simulated NAO index (across historical, hist-nat, hist-GHG, and hist-aer ensembles) shifted from neutral or negative before 1970 to positive and significant afterwards.

Our approach corroborates these findings, suggesting CMIP6 models are better at reproducing recent NAO patterns, even in piControl runs. This indicates that the bias originates from intrinsic model variability. However, the NAO-C3 overestimation decreases as higher levels of GHG forcing are applied in future scenarios (Figure 8). Between historical and ssp585, the NAO-C3 bias is halved, suggesting that anthropogenic forcing could improve the skill of models in capturing NAO shifts. This signal also appears when comparing the results for hist-nat and hist-GHG, although it is weaker.

A critical issue is how these biases impact precipitation projections in Europe. Our analysis confirms that CMIP6 datasets can replicate observed NAO variations and their precipitation effects (Figures 9 and 10). However, the overestimation of NAO-C3 suggests an overrepresentation of associated atmospheric dynamics, intensifying the modulation of NAO over northwestern and

southwestern Europe. Beyond the potential consequences for the total projected precipitation, which are complex to conclude due to the many sources of uncertainty in climate models, the most important point is that when working with the NAO in future projections, it is not always assumed that its modulation may vary across different time periods. This calls into question studies that evaluate future precipitation changes solely based on NAO state or compare historical and future periods without accounting for NAO's long-term variability. Promisingly, experiments forcing NAO's multidecadal variability to match observations (Schurer *et al.*, 2023) offer a pathway to improve model assimilation of NAO fluctuations. These could enhance understanding of ocean–atmosphere linkages and enable assessments of NAO dynamics under projected 21st-century forcings.

5 | CONCLUSIONS

This study analyzed long-term NAO fluctuations during the Industrial Era, addressing the AR6 IPCC call to enhance understanding of NAO multidecadal variability. Using a clustering method based on gradient (g) and mean flux direction (fd) implicit in NAO, 135 consecutive 30-year periods were evaluated. The study also assessed the influence of these fluctuations on European precipitation and compared observations with CMIP6 simulations. Key findings include:

1. Three distinct NAO patterns were identified: NAO-C1 (Iceland–Italy), NAO-C2 (Iceland–Azores), and NAO-C3 (Scandinavia–Azores), each with unique temporal behaviours. These clusters exhibit significant differences in precipitation modulation.
2. Historical CMIP6 simulations replicate all observed NAO clusters, confirming consistency despite limited past observational data. However, the models misinterpret cluster frequencies due to overestimation of the fd metric.
3. These biases, affecting the weighting of NAO patterns, significantly contribute to uncertainties in precipitation projections, particularly for Europe. Accurate reproduction of NAO patterns, as observed in 20CRv3, is critical for reliable regional precipitation assessments. The analysis demonstrates that if the NAO pattern is simulated similarly to the 20CRv3 clusters, its influence on precipitation also varies significantly in climate models. Furthermore, these errors propagate into regional simulations driven by global models.

This study confirms that global climate simulations still fall short in accurately reproducing observed NAO shifts. While they capture large-scale circulation variability and synoptic patterns, their representation is disorganized compared to reanalysis and exhibits random frequency biases. Key ocean–atmosphere feedback, crucial for blocking activity in Greenland, Scandinavia, and the Atlantic Ridge, remains unresolved or misrepresented, raising concerns about the models' capacity to project future NAO–anthropogenic forcing interactions. To address these gaps, ocean-nudging experiments or approaches replicating observed NAO trends should be prioritized to clarify ocean–NAO mechanisms. Additionally, the spatial resolution with which the physical configurations are resolved does not appear to be a key element in the model's skill.

The NAO-C3 pattern observed in recent decades is generally overestimated in simulations, unravelling an intrinsic model configuration bias. Although this study cannot confirm that hypothesis, our findings strongly indicate that the spatiotemporal variability of NAO, as represented in 20CRv3, is better captured in ssp585 simulations with stronger GHG forcing. This suggests that historical runs may fail to alter the state of the atmosphere and ocean as observed in 20CRv3, whereas ssp585 does when GHG concentrations become severe. This does not imply a direct attribution of NAO-C3 characteristics to GHG forcing but rather highlights multiple uncertainties related to the ability of climate models to reproduce NAO. These uncertainties stem from factors ranging from the fundamental physical configuration of the models to the assimilation of forcings.

Given the established influence of ocean dynamics on NAO variability – through mechanisms such as atmospheric blocking, jet stream circulation, and others – it is possible that the underestimation of GHG forcing primarily affects the ocean rather than the atmosphere. These open questions highlight several promising directions for future research with potential high impact on the scientific community and could significantly enhance future CMIP7 global models.

ACKNOWLEDGEMENTS

This study was supported by the Spanish Ministry of Science, Innovation and Universities–Agencia Estatal de Investigación and the European Regional Development Fund (MCI/AEI/FEDER, UE) through the projects ECCE and ONFIRE (grant nos PID2020-115693RB-I00 and PID2021-123193OB-I00). A. Halifa-Marín is grateful for his MCI/AEI predoctoral contract (FPU18/00824). M. Turco acknowledges funding by the MCI/AEI Ramón y Cajal Grant Reference RYC2019-027115-I. Finally, we are very grateful to both anonymous reviewers who provided key suggestions to improve the scientific quality of this article.

CONFLICT OF INTEREST STATEMENT

The authors declare that they have no conflict of interest.

DATA AVAILABILITY STATEMENT

All data used in this study are publicly available online. For 20CRv3 reanalysis, 80-member ensemble (https://psl.noaa.gov/data/gridded/data.20thC_ReanV3.html) and 80 members (https://oldweather.github.io/20CRv3-diagnostics/stripes/PRATE/data.html); for ERA5 (https://cds.climate.copernicus.eu); for ERA20C (https://www.ecmwf.int/en/forecasts/dataset/ecmwf-reanalysis-20th-century); for NCEP Reanalysis 1 (https://psl.noaa.gov/data/gridded/data.ncep.reanalysis.html); for Greenland Blocking Index (https://psl.noaa.gov/gcos_wgsp/Timeseries/GBI_UL/) and Atlantic Multidecadal Oscillation Index (https://climatedataguide.ucar.edu/climate-data/atlantic-multi-decadal-oscillation-amo); for CMIP6 experiments (https://esgf-data.dkrz.de/search/cmip6-dkrz/); for CMIP5 experiments (https://aims2.llnl.gov/search/cmip5/); and for precipitation observations in Europa (Vicente-Serrano *et al.*, 2021, https://doi.org/10.1002/joc.6719; upon request).

REFERENCES

Birkel, S.D., Mayewski, P.A., Maasch, K.A., Kurbatov, A.V. & Lyon, B. (2018) Evidence for a volcanic underpinning of the Atlantic multidecadal oscillation. *Npj Climate and Atmospheric Science*, 1(1), 24. Available from: https://doi.org/10.1038/s41612-018-0036-6

Börgel, F., Frauen, C., Neumann, T. & Meier, H. (2020) The Atlantic multidecadal oscillation controls the impact of the North Atlantic oscillation on north European climate. *Environmental Research Letters*, 15(10), 104025. Available from: https://doi.org/10.1088/1748-9326/aba925

Börgel, F., Meier, H.M., Gröger, M., Rhein, M., Dutheil, C. & Kaiser, J.M. (2022) Atlantic multidecadal variability and the implications for north European precipitation. *Environmental Research Letters*, 17(4), 44040. Available from: https://doi.org/10.1088/1748-9326/ac5ca1

Boucher, O., Servonnat, J., Albright, A.L., Aumont, O., Balkanski, Y., Bastrikov, V. et al. (2020) Presentation and evaluation of the IPSL-CM6A-LR climate model. *Journal of Advances in Modeling Earth Systems*, 12(7), e2019MS002010. Available from: https://doi.org/10.1029/2019MS002010

Bracegirdle, T.J. (2022) Early-to-late Winter 20th century North Atlantic multidecadal atmospheric variability in observations, CMIP5 and CMIP6. *Geophysical Research Letters*, 49(11), e2022GL098212. Available from: https://doi.org/10.1029/2022GL098212

Campitelli, E. (2021) metR: tools for easier analysis of meteorological fields. https://doi.org/10.5281/zenodo.2593516

Campitelli, E., Díaz, L.B. & Vera, C. (2022) Assessment of zonally symmetric and asymmetric components of the southern annular mode using a novel approach. *Climate Dynamics*, 58, 161–178. Available from: https://doi.org/10.1007/s00382-021-05896-5

Christiansen, B., Yang, S. & Matte, D. (2022) The forced response and decadal predictability of the North Atlantic oscillation: nonstationary and fragile skills. *Journal of Climate*, 35(18), 5869–5882. Available from: https://doi.org/10.1175/JCLI-D-21-0807.1

CMIP. (2024) Coupled Model Intercomparison Project - Data Access. Developed by WCRP. Retrieved from https://wcrp-cmip.org/cmip-data-access/, last access: 9 December 2024.

Comas-Bru, L. & McDermott, F. (2014) Impacts of the EA and SCA patterns on the European twentieth century NAO-winter climate relationship. *Quarterly Journal of the Royal Meteorological Society*, 140(679), 354–363. Available from: https://doi.org/10.1002/qj.2158

Cresswell-Clay, N., Ummenhofer, C., Thatcher, D., Wanamaker, A., Denniston, R., Asmerom, Y. et al. (2022) Twentieth-century Azores high expansion unprecedented in the past 1,200 years. *Nature Geoscience*, 15, 548–553. Available from: https://doi.org/10.1038/s41561-022-00971-w

Deser, C., Lehner, F., Rodgers, K.B., Ault, T., Delworth, T.L., DiNezio, P.N. et al. (2020) Insights from earth system model initial-condition large ensembles and future prospects. *Nature Climate Change*, 10, 277–286. Available from: https://doi.org/10.1038/s41558-020-0731-2

Ditlevsen, P. & Ditlevsen, S. (2023) Warning of a forthcoming collapse of the Atlantic meridional overturning circulation. *Nature Communications*, 14(1), 4254. Available from: https://doi.org/10.1038/s41467-023-39810-w

Dorrington, J., Strommen, K. & Fabiano, F. (2022) Quantifying climate model representation of the wintertime euro-Atlantic circulation using geopotential-jet regimes. *Weather and Climate Dynamics*, 3, 505–533. Available from: https://doi.org/10.5194/wcd-3-505-2022

Döscher, R., Acosta, M., Alessandri, A., Anthoni, P., Arsouze, T., Bergman, T. et al. (2022) The EC-Earth3 earth system model for the coupled model Intercomparison project 6. *Geoscientific Model Development*, 15, 2973–3020. Available from: https://doi.org/10.5194/gmd-15-2973-2022

Eade, R., Stephenson, D., Scaife, A. & Smith, D. (2022) Quantifying the rarity of extreme multi-decadal trends: how unusual was the late twentieth century trend in the North Atlantic oscillation? *Climate Dynamics*, 58(5), 1555–1568. Available from: https://doi.org/10.1007/s00382-021-05978-4

Eyring, V., Gillett, N., Rao, K.A., Barimalala, R., Parrillo, M.B., Bellouin, N. et al. (2021) Human influence on the climate system. In: Masson-Delmotte, V., Zhai, P., Pirani, A., Connors, S., Péan, C., Berger, S. et al. (Eds.) *Climate change 2021: the physical science basis*. Cambridge and New York: Cambridge University Press, pp. 423–552. Available from: https://doi.org/10.1017/9781009157896.005

Fasullo, J.T., Phillips, A.S. & Deser, C. (2020) Evaluation of leading modes of climate variability in the CMIP archives. *Journal of Climate*, 33(13), 5527–5545. Available from: https://doi.org/10.1175/JCLI-D-19-1024.1

Fuentes-Franco, R., Docquier, D., Koenigk, T., Zimmermann, K. & Giorgi, F. (2023) Winter heavy precipitation events over northern Europe modulated by a weaker NAO variability by the end of the 21st century. *Npj Climate and Atmospheric Science*, 6(1), 72. Available from: https://doi.org/10.1038/s41612-023-00396-1

Grise, K.M. & Davis, S.M. (2020) Hadley cell expansion in CMIP6 models. *Atmospheric Chemistry and Physics*, 20(9), 5249–5268. Available from: https://doi.org/10.5194/acp-20-5249-2020

Gulev, S., Thorne, P., Ahn, J., Dentener, F., Domingues, C., Gerland, S. et al. (2021) Changing state of the climate system. In:

Masson-Delmotte, V., Zhai, P., Pirani, A., Connors, S., Péan, C., Berger, S. et al. (Eds.) *Climate change 2021: the physical science basis*. Cambridge and New York: Cambridge University Press, pp. 287–422. Available from: https://doi.org/10.1017/9781009157896.004

Hajima, T., Watanabe, M., Yamamoto, A., Tatebe, H., Noguchi, M.A., Abe, M. et al. (2020) Development of the MIROC-ES2L earth system model and the evaluation of biogeochemical processes and feedbacks. *Geoscientific Model Development*, 13, 2197–2244. Available from: https://doi.org/10.5194/gmd-13-2197-2020

Halifa-Marín, A., Pravia-Sarabia, E., Torres Vázquez, M.A., Trigo, R., Vicente-Serrano, S.M., Jerez, S. et al. (2025) Unparalleled EA-like leading mode of variability in the early 20th century highlights the need for understanding non-stationarity in the North Atlantic climate system. *Atmospheric Research*, 314, 107796. Available from: https://doi.org/10.1016/j.atmosres.2024.107796

Hanna, E., Cropper, T., Hall, R. & Cappelen, J. (2016) Greenland blocking index 1851–2015: a regional climate change signal. *International Journal of Climatology*, 36(15), 4847–4861. Available from: https://doi.org/10.1002/joc.4673

Hernández, A., Martin-Puertas, C., Moffa-Sánchez, P., Moreno-Chamarro, E., Ortega, P., Blockley, S. et al. (2020) Modes of climate variability: synthesis and review of proxy-based reconstructions through the Holocene. *Earth-Science Reviews*, 209, 103286. Available from: https://doi.org/10.1016/j.earscirev.2020.103286

Hersbach, H., Bell, B., Berrisford, P., Hirahara, S., Horányi, A., Muñoz-Sabater, J. et al. (2020) The ERA5 global reanalysis. *Quarterly Journal of the Royal Meteorological Society*, 146(730), 1999–2049. Available from: https://doi.org/10.1002/qj.3803

Hu, H., Trouet, V., Spötl, C., Tsai, H.-C., Chien, W.-Y., Sung, W.-H. et al. (2022) Tracking westerly wind directions over Europe since the middle Holocene. *Nature Communications*, 13(1), 7866. Available from: https://doi.org/10.1038/s41467-022-34952-9

Huang, B.Y., Thorne, P.W., Banzon, V.F. et al. (2017) Extended Reconstructed Sea surface temperature, version 5 (ERSSTv5): upgrades, validations, and intercomparisons. *Journal of Climate*, 30, 8179–8205. Available from: https://doi.org/10.1175/JCLI-D-16-0806.1

Hurrell, J.W., Kushnir, Y., Ottersen, G. & Visbeck, M. (2003) An overview of the north atlantic oscillation. *Geophysical Monograph-American Geophysical Union*, 134, 1–36. Available from: https://doi.org/10.1029/134GM01

Kalnay, E., Kanamitsu, M., Kistler, R., Collins, W., Deaven, D., Gandin, L. et al. (1996) The NCEP/NCAR 40-year reanalysis project. *Bulletin of the American Meteorological Society*, 77, 437–471. Available from: https://doi.org/10.1175/1520-0477(1996)077<0437:TNYRP>2.0.CO;2

Kim, H.J., An, S.-I. & Kim, D. (2021) Timescale-dependent AMOC-AMO relationship in an earth system model of intermediate complexity. *International Journal of Climatology*, 41, E3298–E3306. Available from: https://doi.org/10.1002/joc.6926

Knudsen, M.F., Jacobsen, B.H., Seidenkrantz, M.-S. & Olsen, J. (2014) Evidence for external forcing of the Atlantic multidecadal oscillation since termination of the Little ice age. *Nature Communications*, 5(1), 3323. Available from: https://doi.org/10.1038/ncomms4323

Kwon, Y.-O., Seo, H.-S., Ummenhofer, C.C. & Joyce, T.M. (2020) Impact of multidecadal variability in Atlantic SST on winter atmospheric blocking. *Journal of Climate*, 33(3), 867–892. Available from: https://doi.org/10.1175/JCLI-D-19-0324.1

Latif, M., Sun, J., Visbeck, M. & Bordbar, M.H. (2022) Natural variability has dominated Atlantic meridional overturning circulation since 1900. *Nature Climate Change*, 12(5), 455–460. Available from: https://doi.org/10.1038/s41558-022-01342-4

Lehmann, J. & Coumou, D. (2015) The influence of mid-latitude storm tracks on hot, cold, dry and wet extremes. *Scientific Reports*, 5, 17491. Available from: https://doi.org/10.1038/srep17491

Lionello, P., D'Agostino, R., Ferreira, D., Nguyen, H. & Singh, M. S. (2024) The Hadley circulation in a changing climate. *Annals of the New York Academy of Sciences*, 1534(1), 69–93. Available from: https://doi.org/10.1111/nyas.15114

Mann, M.E., Steinman, B.A., Brouillette, S.A. & Miller, S.K. (2021) Multidecadal climate oscillations during the past millennium driven by volcanic forcing. *Science*, 371(6533), 1014–1019. Available from: https://doi.org/10.1126/science.abc5810

Mauritsen, T., Bader, J., Becker, T., Behrens, J., Bittner, M., Brokopf, R. et al. (2019) Developments in the MPI-M earth system model version 1.2 (MPI-ESM1.2) and its response to increasing CO_2. *Journal of Advances in Modeling Earth Systems*, 11(4), 998–1038. Available from: https://doi.org/10.1029/2018MS001400

McGregor, H.V., Evans, M.N., Goosse, H., Leduc, G., Martrat, B., Addison, J.A. et al. (2015) Robust global ocean cooling trend for the pre-industrial common era. *Nature Geoscience*, 8(9), 671–677. Available from: https://doi.org/10.1038/ngeo2510

Mellado-Cano, J., Barriopedro, D., García-Herrera, R., Trigo, R. & Hernández, A. (2019) Examining the North Atlantic oscillation, East Atlantic pattern, and jet variability since 1685. *Journal of Climate*, 32(19), 6285–6298. Available from: https://doi.org/10.1175/JCLI-D-19-0135.1

Miller, R.L., Schmidt, G.A., Nazarenko, L.S., Bauer, S.E., Kelley, M., Ruedy, R. et al. (2021) CMIP6 historical simulations (1850–2014) with GISS-E2.1. *Journal of Advances in Modeling Earth Systems*, 13(1), e2019MS002034. Available from: https://doi.org/10.1029/2019MS002034

Moore, G., Renfrew, I. & Pickart, R. (2013) Multidecadal mobility of the North Atlantic oscillation. *Journal of Climate*, 26(8), 2453–2466. Available from: https://doi.org/10.1175/JCLI-D-12-00023.1

Müller, W.A., Jungclaus, J.H., Mauritsen, T., Baehr, J., Bittner, M., Budich, R. et al. (2018) A higher-resolution version of the max planck institute earth system model (MPI-ESM1.2-HR). *Journal of Advances in Modeling Earth Systems*, 10(7), 1383–1413. Available from: https://doi.org/10.1029/2017MS001217

Oltmanns, M., Karstensen, J., Moore, G.W.K. & Josey, S.A. (2020) Rapid cooling and increased storminess triggered by freshwater in the North Atlantic. *Geophysical Research Letters*, 47(14), e2020GL087207. Available from: https://doi.org/10.1029/2020GL087207

Omrani, N.-E., Keenlyside, N., Matthes, K., Boljka, L., Zanchettin, D., Jungclaus, J.H. et al. (2022) Coupled stratosphere-troposphere-Atlantic multidecadal oscillation and its importance for near-future climate projection. *Npj Climate and Atmospheric Science*, 5(1), 59. Available from: https://doi.org/10.1038/s41612-022-00275-1

Poli, P., Hersbach, H., Dee, D., Berrisford, P., Simmons, A., Vitart, F. et al. (2016) ERA-20C: An atmospheric reanalysis of the twentieth century. *Journal of Climate*, 29(11), 4083–4097. Available from: https://doi.org/10.1175/JCLI-D-15-0556.1

Rayner, N., Parker, D.E., Horton, E., Folland, C.K., Alexander, L.V., Rowell, D. et al. (2003) Global analyses of sea surface temperature, sea ice, and night marine air temperature since the late nineteenth century. *Journal of Geophysical Research: Atmospheres*, 108(D14), 2002JD002670. Available from: https://doi.org/10.1029/2002JD002670

Rimbu, N., Lohmann, G. & Ionita, M. (2014) Interannual to multidecadal euro–Atlantic blocking variability during winter and its relationship with extreme low temperatures in Europe. *Journal of Geophysical Research: Atmospheres*, 119(24), 13–621. Available from: https://doi.org/10.1002/2014JD021983

Schiemann, R., Athanasiadis, P., Barriopedro, D., Doblas-Reyes, F., Lohmann, K., Roberts, M.J. et al. (2020) Northern hemisphere blocking simulation in current climate models: evaluating progress from the climate model Intercomparison project phase 5 to 6 and sensitivity to resolution. *Weather and Climate Dynamics*, 1(1), 277–292. Available from: https://doi.org/10.5194/wcd-1-277-2020

Schurer, A.P., Hegerl, G.C., Goosse, H., Bollasina, M.A., England, M.H., Smith, D.M. et al. (2023) Role of multi-decadal variability of the winter North Atlantic oscillation on northern hemisphere climate. *Environmental Research Letters*, 18(4), 44046. Available from: https://doi.org/10.1088/1748-9326/acc477

Sellar, A.A., Walton, J., Jones, C.G., Wood, R., Abraham, N.L., Andrejczuk, M. et al. (2020) Implementation of UK earth system models for CMIP6. *Journal of Advances in Modeling Earth Systems*, 12(4), e2019MS001946. Available from: https://doi.org/10.1029/2019MS001946

Sigmond, M., Anstey, J., Arora, V., Digby, R., Gillett, N., Kharin, V. et al. (2023) Improvements in the Canadian earth system model (CanESM) through systematic model analysis: CanESM5.0 and CanESM5.1. *Geoscientific Model Development*, 16, 6553–6591. Available from: https://doi.org/10.5194/gmd-16-6553-2023

Singh, H.K., Hakim, G.J., Tardif, R., Emile-Geay, J. & Noone, D.C. (2018) Insights into Atlantic multidecadal variability using the last millennium reanalysis framework. *Climate of the Past*, 14(2), 157–174. Available from: https://doi.org/10.5194/cp-14-157-2018

Slivinski, L., Compo, G., Sardeshmukh, P., Whitaker, J., McColl, C., Allan, R. et al. (2021) An evaluation of the performance of the twentieth century reanalysis version 3. *Journal of Climate*, 34(4), 1417–1438. Available from: https://doi.org/10.1175/JCLI-D-20-0505.1

Smith, D., Scaife, A., Eade, R., Athanasiadis, P., Bellucci, A., Bethke, I. et al. (2020) North Atlantic climate far more predictable than models imply. *Nature*, 583(7818), 796–800. Available from: https://doi.org/10.1038/s41586-020-2525-0

Swart, N.C., Cole, J.N., Kharin, V.V., Lazare, M., Scinocca, J.F., Gillett, N.P. et al. (2019) The Canadian earth system model version 5 (CanESM5.0.3). *Geoscientific Model Development*, 12(11), 4823–4873. Available from: https://doi.org/10.5194/gmd-12-4823-2019

Tatebe, H., Ogura, T., Nitta, T., Komuro, Y., Ogochi, K., Takemura, T. et al. (2019) Description and basic evaluation of simulated mean state, internal variability, and climate sensitivity in MIROC6. *Geoscientific Model Development*, 12(7), 2727–2765. Available from: https://doi.org/10.5194/gmd-12-2727-2019

Trenberth, K.E. & Shea, D.J. (2006) Atlantic hurricanes and natural variability in 2005. *Geophysical Research Letters*, 33, L12704. Available from: https://doi.org/10.1029/2006gl026894

Tsanis, I. & Tapoglou, E. (2019) Winter North Atlantic oscillation impact on European precipitation and drought under climate change. *Theoretical and Applied Climatology*, 135, 323–330. Available from: https://doi.org/10.1007/s00704-018-2379-7

Vicente-Serrano, S.M., Domínguez-Castro, F., Murphy, C., Hannaford, J., Reig, F., Peña-Angulo, D. et al. (2021) Long-term variability and trends in meteorological droughts in Western Europe (1851–2018). *International Journal of Climatology*, 41, E690–E717. Available from: https://doi.org/10.1002/joc.6719

Vicente-Serrano, S.M. & López-Moreno, J.I. (2008) Nonstationary influence of the North Atlantic oscillation on European precipitation. *Journal of Geophysical Research: Atmospheres*, 113(D20), 2008JD010382. Available from: https://doi.org/10.1029/2008JD010382

Voldoire, A., Saint-Martin, D., Sénési, S., Decharme, B., Alias, A., Chevallier, M. et al. (2019) Evaluation of CMIP6 deck experiments with CNRM-CM6-1. *Journal of Advances in Modeling Earth Systems*, 11(7), 2177–2213. Available from: https://doi.org/10.1029/2019MS001683

Walker, J.S., Kopp, R.E., Little, C.M. & Horton, B.P. (2022) Timing of emergence of modern rates of sea-level rise by 1863. *Nature Communications*, 13(1), 966. Available from: https://doi.org/10.1038/s41467-022-28564-6

Wang, Y., Magnusdottir, G., Stern, H., Tian, X. & Yu, Y. (2012) Decadal variability of the NAO: introducing an augmented NAO index. *Geophysical Research Letters*, 39(21), 2012GL053413. Available from: https://doi.org/10.1029/2012GL053413

Woollings, T., Franzke, C., Hodson, D.L., Dong, B., Barnes, E.A., Raible, C.C. et al. (2015) Contrasting interannual and multidecadal NAO variability. *Climate Dynamics*, 45, 539–556. Available from: https://doi.org/10.1007/s00382-014-2237-y

Wu, M., Li, C. & Zhang, Z. (2024) Recalibrated projections of the Hadley circulation under global warming. *Environmental Research Letters*, 19(10), 104041. Available from: https://doi.org/10.1088/1748-9326/ad751f

Ziehn, T., Chamberlain, M.A., Law, R.M., Lenton, A., Bodman, R.W., Dix, M. et al. (2020) The Australian earth system model: ACCESS-ESM1.5. *Journal of Southern Hemisphere Earth Systems Science*, 70(1), 193–214. Available from: https://doi.org/10.1071/ES19035

SUPPORTING INFORMATION

Additional supporting information can be found online in the Supporting Information section at the end of this article.

How to cite this article: Halifa-Marín, A., Torres-Vázquez, M.A., Trigo, R., Vicente-Serrano, S.M., Turco, M., Jiménez-Guerrero, P. *et al.* (2025) Too-stable North Atlantic climate system in CMIP6 experiments undermines precipitation projections in Europe. *Quarterly Journal of the Royal Meteorological Society*, e4999. Available from: https://doi.org/10.1002/qj.4999